

Graph Topology Learning Under Privacy Constraints

Xiang Zhang, *Student Member, IEEE*,

Abstract—We consider the problem of inferring the underlying graph topology from smooth graph signals in a novel but practical scenario where data are located in distributed clients and are privacy-sensitive. The main difficulty of this task lies in how to utilize the data of all isolated clients—which may be heterogeneous—under privacy constraints. Towards this end, we propose a framework where personalized graphs for local clients as well as a consensus graph are jointly learned. The personalized graphs match local data distributions, thereby mitigating data heterogeneity, while the consensus graph captures the global information. We next devise a tailored algorithm to solve the induced problem without violating privacy constraints, i.e., all private data are processed locally. To further enhance privacy protection, we introduce differential privacy (DP) into the proposed algorithm to resist privacy attacks when transmitting model updates. Theoretically, we establish provable convergence analyses for the proposed algorithms, including that with DP. Finally, extensive experiments on both synthetic and real-world data are carried out to validate the proposed framework. Experimental results illustrate that our approach can learn graphs effectively in the target scenario.

Index Terms—Graph learning, federated learning, differential privacy, graph signal processing, privacy-preserving algorithm

I. INTRODUCTION

Graphs are powerful tools for characterizing structured data since the relationships between data entities can be flexibly described by graphs [1]. Some celebrated graph-based models, e.g., spectral clustering [2] and graph neural networks [3], have been extensively applied in many fields. Among these applications, a graph that accurately represents the information inherent in the structured data is required, which, however, is not available in many cases. An alternative approach is to learn graphs directly from raw data, termed graph learning, for downstream tasks [1], [4]. Recently, with the rise of graph signal processing (GSP) [5], various approaches attempt to learn graphs from a signal processing perspective. One of the most studied GSP-based models—smoothness-based model—postulates that the observed graph signals are smooth over the graph to be learned [6], [7]. Intuitively, a graph signal being smooth means that the signal values corresponding to two connected nodes of the underlying graphs are similar [7]. Typically, learning graphs from smooth signals is equivalent to minimizing a constrained quadratic Laplacian form problem, where the quadratic Laplacian form is related to signal smoothness, and the constraints (regularizers) are used to assign properties to the graphs, such as sparsity [6] and node connectivity [7]. Many signals appear to be smooth over their underlying graph, such as meteorology data [6] and medicine data [8], implying numerous applications of smoothness-based graph learning models.

The author is with the School of Information Science and Engineering, Southeast University, Nanjing 210096, China (e-mail: xiangzhang369@seu.edu.cn).

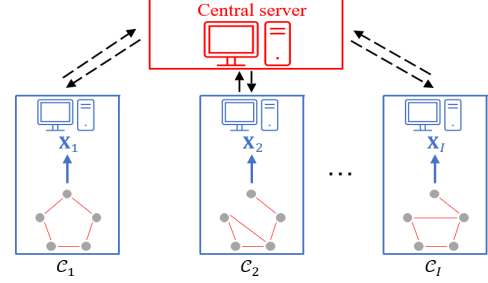


Fig. 1: The illustration of the target scenario. The clients C_1, \dots, C_I store graphs signals X_1, \dots, X_I generated from I distinct but related graphs. The data are not allowed to leave their clients, but all clients can commute with a central server.

Here, we consider learning graphs in a previously unexplored scenario, where data are stored across different clients (e.g., companies and organizations) and are privacy-sensitive. This scenario is known as data silos [9], and a typical example is medical data. Suppose some hospitals collect brain fMRI data from autistic and non-autistic individuals separately to learn the impact of autism on connectivity networks of brain functional regions [8]. However, the data are prohibited from leaving the hospital where they are stored as people are reluctant to disclose their private data. Data silos prevent us from learning graphs using data from all clients, resulting in poor learning performance. Thus, it is essential to develop an approach that can learn graphs under privacy constraints. Nevertheless, the task is not trivial, and the first challenge is how to leverage data information from all clients without violating privacy constraints. Furthermore, the graph signals across different silos are inherently non-IID due to factors such as different data collection protocols and heterogeneous underlying graphs [10]. We still use the brain fMRI data as an example. The brain functional connectivity networks of autistic and non-autistic individuals are different due to the impact of autism. It is unreasonable to utilize heterogeneous data to learn a single global graph like traditional paradigms [6], [7]. Thus, the second challenge is handling heterogeneous data.

Regarding the first challenge, federated learning (FL) [11]–[13] is an emerging tool for learning models based on datasets distributed across multiple clients under privacy constraints. The primary feature of FL is that clients transmit model updates instead of raw data to a central server to collaboratively learn a global model [11]. Privacy can be preserved in this schema to some extent since all data are processed locally [12]. However, standard FL algorithms such as FedAvg [14] learn a single global model from all data, which may suffer from performance degradation when data are non-IID. A widely used approach to handle data heterogeneity—the second challenge—is personalized FL (PFL) [15]. The philosophy behind PFL is that we learn for each client a personalized model

that matches its data distribution to mitigate the impact of heterogeneity. The techniques for adapting global models for individual clients include transfer learning [16], multi-task learning [17], and meta-learning [18].

Borrowing ideas from PFL, we learn a personalized graph for each local client to handle data heterogeneity. However, it poses additional challenges due to the characteristics of graph learning tasks. (i) Our goal is to jointly learn all local graphs by exploiting their latent relationships so that each local graph benefits from "borrowing" information from other datasets. Thus, it is crucial to describe the relationships between local graphs, which is the focus of multiple graph learning (MGL). The common approach of MGL models is to design regularization penalties, e.g., fused Lasso penalty [19], group Lasso penalty [20], Gram matrix-based penalty [21], and those describing temporally topological relationships [22]–[25], etc. These regularizers characterize topological relationships among multiple graphs, but few of them consider capturing common structures from all local graphs. In practice, many graphs share common structures, one of which is multimedia data collected from various input channels, such as photos of the same object taken from different angles. These photos have the same semantic details since they are from the same object [26]. The common structures reflect the global information across all local datasets, which may be useful for many downstream tasks. (ii) It is infeasible to apply existing PFL algorithms, such as [17], [27]–[30], to our task because their personalization methods do not fit the problem of concern. On the other hand, privacy-constrained graph learning problems can be categorized as cross-silo FL, where clients are a few companies or organizations rather than massive mobile devices in cross-device FL [11], [14]. Consequently, a tailored privacy-preserving algorithm is required to learn graphs in the target scenario. (iii) Although the standard FL(PFL) framework has taken a step towards preserving privacy, eavesdroppers may still steal users' private information through methods such as model inversion attacks [31] and membership inference attacks [32]. A widely used technique that is resistant to most privacy attacks when transferring model updates is differential privacy (DP) [33], which preserves privacy by adding artificial noise to ensure that the estimated output is indistinguishable whether or not a particular user's data is considered [34]. Albeit promising, the added noise requires careful calibration to meet a certain level of DP, especially for our graph learning models and tailored algorithms.

To address these issues, we propose a framework to learn graphs from smooth but heterogeneous data under privacy constraints. Our contributions can be summarized as follows:

- We propose an MGL model in which multiple local personalized graphs and a consensus graph are jointly learned. The consensus graph can capture the global information across all datasets, while the local graphs preserve the heterogeneity of local datasets.
- We devise a privacy-preserving algorithm to learn graphs under privacy constraints. The algorithm follows the communication protocol of FL to alternately update the personalized graphs in local clients and the consensus graph in the central server. Furthermore, we introduce

DP into the proposed algorithm to prevent privacy attacks by adding artificial noise calibrated with strict theoretical guarantees to published data.

- We provide convergence analyses of the proposed algorithms, which are not straightforward and differ from existing works due to the specificity of our algorithms. The results illustrate that the convergence rate of our algorithms is $\mathcal{O}(1/T)$, where T is the number of iterations. Besides, the algorithm with DP bears a constant bias determined by the added noise.
- Extensive experiments with synthetic and real-world data are conducted to validate our framework, and the results show that our approach can effectively learn graphs under privacy constraints.

Organization: The rest of this paper is organized as follows. We start with background information and the problem of concern in Section II. The proposed framework for learning graphs in the target scenario is presented in III, followed by the algorithm with DP in Section IV. Experimental setups and results are provided in Section V. Finally, concluding remarks are presented in Section VI.

Notations: Throughout this paper, vectors, matrices, and sets are written in bold lowercase letters, bold uppercase letters, and calligraphic uppercase letters, respectively. Given a vector \mathbf{y} and matrix \mathbf{Y} , $\mathbf{y}[i]$ and $\mathbf{Y}[ij]$ are the i -th entry of \mathbf{y} and the (i, j) entry of \mathbf{Y} . The vectors $\mathbf{1}$, $\mathbf{0}$, and matrix \mathbf{I} represent all-one vectors, all-zero vectors, and identity matrices, respectively. The ℓ_1 , ℓ_2 , and Frobenius norm are represented $\|\cdot\|_1$, $\|\cdot\|_2$ and $\|\cdot\|_F$, respectively. The notations \circ , \dagger , $\text{Tr}(\cdot)$, and $\text{Pr}(\cdot)$ stand for Hadamard product, pseudo inverse, trace operator and taking probability, respectively. For a set \mathcal{Y} , $\text{conv}[\mathcal{Y}]$ is the affine and convex hulls of \mathcal{Y} . Moreover, $\text{diag}(\mathbf{y})$, $\text{diag}(\mathbf{Y})$, and $\text{diag}_0(\mathbf{Y})$ mean converting vector \mathbf{y} to a diagonal matrix, converting the diagonal elements of \mathbf{Y} to a vector, and setting the diagonal entries of \mathbf{Y} to 0. Finally, \mathbb{R} and \mathbb{S} represent the domain of real values and symmetric matrices whose dimensions depend on the context.

II. BACKGROUND AND PROBLEM STATEMENT

A. GSP Background

We consider undirected graphs with non-negative weights and no self-loops. For such a graph $\mathcal{G}(\mathcal{V}, \mathcal{E})$ with d vertices, where \mathcal{V} and \mathcal{E} are the sets of vertices and edges, respectively, its adjacency matrix $\mathbf{W} \in \mathbb{S}^{d \times d}$ is a symmetric matrix with zero diagonal entries and non-negative off-diagonal entries. The Laplacian matrix of \mathcal{G} is defined as $\mathbf{L} = \mathbf{D} - \mathbf{W}$ [35], where the degree matrix $\mathbf{D} \in \mathbb{S}^{d \times d}$ is a diagonal matrix satisfying $\mathbf{D}[ii] = \sum_{j=1}^d \mathbf{W}[ij]$. The matrices \mathbf{W} and \mathbf{L} encode the topology of \mathcal{G} since they have a one-to-one relationship. We study the graph signal $\mathbf{x} = [\mathbf{x}[1], \dots, \mathbf{x}[d]]^\top \in \mathbb{R}^d$ associated with \mathcal{G} , where $\mathbf{x}[i]$ is the signal value of node $i \in \mathcal{V}$. The smoothness of \mathbf{x} over \mathcal{G} is defined as follows.

Definition 1. (Smoothness [6]). Given a graph signal \mathbf{x} and a graph \mathcal{G} whose Laplacian matrix and adjacency matrix are \mathbf{L} and \mathbf{W} , respectively, the smoothness of \mathbf{x} over \mathcal{G} is

$$\mathbf{x}^\top \mathbf{L} \mathbf{x} = \frac{1}{2} \sum_{i,j} \mathbf{W}[ij] (\mathbf{x}[i] - \mathbf{x}[j])^2. \quad (1)$$

The Laplacian quadratic form (1) is known as Dirichlet energy, which quantifies how much the signal \mathbf{x} changes w.r.t. \mathcal{G} . A small value of (1) indicates limited signal variability, meaning that \mathbf{x} is smooth over the corresponding graph [6].

B. Smoothness Based Graph Learning

Given N observations $\mathbf{X} = [\mathbf{x}_1, \dots, \mathbf{x}_N] \in \mathbb{R}^{d \times N}$, smoothness-based graph learning aims to infer graph topology \mathcal{G} under the assumption that the signals \mathbf{X} are smooth over \mathcal{G} . Formally, the problem is written as

$$\min_{\mathbf{L} \in \mathcal{L}} \frac{1}{N} \sum_{n=1}^N \mathbf{x}_n^\top \mathbf{L} \mathbf{x}_n + R(\mathbf{L}), \quad (2)$$

where the first term is to quantify the smoothness of \mathbf{X} over \mathcal{G} , and $R(\mathbf{L})$ is a regularization term that endows \mathcal{G} with desired properties. Here, we follow [7] and select $R(\mathbf{L})$ as $-\alpha \mathbf{1}^\top \log(\text{diag}(\mathbf{L})) + \beta \|\text{diag}_0(\mathbf{L})\|_F^2$, where α and β are predefined constants. The first and second terms of $R(\mathbf{L})$ control node connectivity and edge sparsity of the learned graph, respectively [7]. We use Laplacian matrix \mathbf{L} to represent graph topology of \mathcal{G} , which lies in the set \mathcal{L}

$$\mathcal{L} \triangleq \{\mathbf{L} : \mathbf{L} \in \mathbb{S}^{d \times d}, \mathbf{L}\mathbf{1} = \mathbf{0}, \mathbf{L}[i,j] \leq 0 \text{ for } i \neq j\}. \quad (3)$$

Based on Eq.(1), problem (2) can be rephased as

$$\min_{\mathbf{W} \in \mathcal{A}} \frac{1}{2N} \sum_{n=1}^N \|\mathbf{W} \circ \mathbf{Z}_n\|_1 - \alpha \mathbf{1}^\top \log(\mathbf{W}\mathbf{1}) + \beta \|\mathbf{W}\|_F^2, \quad (4)$$

where $\mathbf{Z}_n \in \mathbb{R}^{d \times d}$ is a pairwise distance matrix defined as

$$\mathbf{Z}_n[i,j] = |\mathbf{x}_n[i] - \mathbf{x}_n[j]|^2. \quad (5)$$

Similarly, \mathcal{A} is the set containing all adjacency matrices,

$$\mathcal{A} = \{\mathbf{W} : \mathbf{W} \in \mathbb{S}^{d \times d}, \mathbf{W} \geq 0, \text{diag}(\mathbf{W}) = \mathbf{0}\}, \quad (6)$$

where $\mathbf{W} \geq 0$ means that all elements of \mathbf{W} are non-negative. By the definition of \mathcal{A} , the number of free variables of \mathbf{W} is $p := \frac{d(d-1)}{2}$ [7]. For simplicity, we define a vector $\mathbf{w} \in \mathbb{R}^p$ whose elements are the upper triangle variables of \mathbf{W} . Then, problem (4) can be rewritten into a vector form as

$$\min_{\mathbf{w} \geq 0} \frac{1}{N} \sum_{n=1}^N \mathbf{z}_n^\top \mathbf{w} - \alpha \mathbf{1}^\top \log(\mathbf{S}\mathbf{w}) + 2\beta \|\mathbf{w}\|_2^2, \quad (7)$$

where \mathbf{S} is a linear operator satisfying $\mathbf{S}\mathbf{w} = \mathbf{W}\mathbf{1}$, and \mathbf{z}_n is the vector form of the upper triangle elements of \mathbf{Z}_n ¹.

C. Problem Statement

As shown in Fig.1, suppose that there are I clients $\mathcal{C}_1, \dots, \mathcal{C}_I$, and the i -th client stores signals $\mathbf{X}_i \in \mathbb{R}^{d \times N_i}$ generated from the local graph \mathcal{G}_i , where N_i is the data size of the i -th dataset. All graphs of different clients are defined over the same node set but may be heterogenous, meaning that the corresponding graph signals may be non-IID. Furthermore, graph signals \mathbf{X}_i are assumed to be smooth over \mathcal{G}_i and are forbidden from leaving the client \mathcal{C}_i due to privacy concerns. However, all clients can exchange information with a third-party central server. Our goal is to learn graphs using heterogeneous data $\mathbf{X}_1, \dots, \mathbf{X}_I$ under privacy constraints.

III. PRIVACY-PRESERVING GRAPH LEARNING

In this section, we first propose an MGL model to learn all local graphs jointly. Then, we devise a privacy-preserving algorithm to solve the induced problem. Finally, the convergence and privacy analysis of the proposed algorithm is provided.

¹The vector \mathbf{z}_n is calculated from \mathbf{x}_n , and hence \mathbf{z}_n is also referred to as observation data in the following sections.

A. Basic Formulation

We use $\mathbf{w}_1, \dots, \mathbf{w}_I$ to represent local graphs $\mathcal{G}_1, \dots, \mathcal{G}_I$, respectively. We assume local graphs have a common structure denoted as \mathbf{w}_{con} . All graphs are then jointly learned via

$$\min_{\mathbf{w}_i \in \mathcal{W}, \mathbf{w}_{\text{con}}} \underbrace{\sum_{i=1}^I \frac{1}{N_i} \sum_{n=1}^{N_i} \mathbf{z}_{i,n}^\top \mathbf{w}_i - \alpha \mathbf{1}^\top \log(\mathbf{S}\mathbf{w}_i + \zeta \mathbf{1})}_{g_i(\mathbf{w}_i)} + 2\beta \|\mathbf{w}_i\|_2^2 + \frac{\rho}{2} \sum_{i=1}^I \gamma_i \|\mathbf{w}_i - \mathbf{w}_{\text{con}}\|_2^2 + \lambda \|\mathbf{w}_{\text{con}}\|_1, \quad (8)$$

where $\mathbf{z}_{i,n}$ is the n -th observed data in client \mathcal{C}_i , ζ is a small enough constant to avoid zero node degree, and $\mathcal{W} := \{\mathbf{w} : \mathbf{w} \geq 0\}$. The term $g_i(\mathbf{w}_i)$ represents the classic smoothness-based graph learning model (7) in \mathcal{C}_i . The term related to $\|\mathbf{w}_i - \mathbf{w}_{\text{con}}\|_2^2$ is used to measure the difference between \mathbf{w}_i and \mathbf{w}_{con} . Constant ρ is the global regularization parameter, while γ_i is the local weight parameter of the similarity between \mathbf{w}_i and \mathbf{w}_{con} . In [36], all local weights, $\gamma_1, \dots, \gamma_I$, have the same value. In our model, we leverage a strategy called inverse distance weighting schema [37] to determine local weights, where γ_i is adaptively adjusted according to the similarity between \mathbf{w}_i and \mathbf{w}_{con} ; see Section III-B for more details. We add the ℓ_1 norm term in (8) because \mathbf{w}_{con} is expected to be sparse, which can remove redundant noisy edges [38]. We use λ to control the sparsity of the consensus graph. The parameters of problem (8) are α, β, ρ , and λ . However, as stated in [7], tuning the importance of the log-degree term w.r.t. the other graph terms has a scaling effect. We can fix α as a constant and search for the other parameters. Therefore, the free parameters of our model are β, ρ and λ . In Section V, we experimentally show that λ can hardly affect local graphs and is easy to tune.

The proposed model (8) enjoys the following advantages. Firstly, our model provides a way to learn graphs of different clients jointly. Compared to learning graphs independently, our model utilizes the information from all datasets, which may boost learning performance. Secondly, we learn a personalized graph for each client, which alleviates the bias of learning a single global graph in the case of data heterogeneity. Lastly, unlike most PFL methods that only learn personalized local models [15], our model learns a consensus graph reflecting global information. Our model differs from [36]—the only work we can find that learns a common structure from multiple graphs—in two ways. First, our model can adaptively adjust the contributions of local graphs to the consensus graph. Second, we consider data privacy while [36] collects all data in a central server.

B. Algorithm

We propose a privacy-preserving algorithm to solve (8), which consists of two steps: (i) updating \mathbf{w}_i in the local client $\mathcal{C}_i, i = 1, \dots, I$, and (ii) updating $\gamma = [\gamma_1, \dots, \gamma_I]^\top \in \mathbb{R}^I$ and \mathbf{w}_{con} in the central server. The complete flow is displayed in Algorithm 1.

Updating \mathbf{w}_i in the local client \mathcal{C}_i : The update corresponds to lines 3-8 in Algorithm 1. In the t -th communication round, \mathcal{C}_i first receives $\mathbf{w}_{\text{con}}^{(t)}$ and $\gamma_i^{(t)}$ from the central server. Let

$f_i(\mathbf{w}_i, \mathbf{w}_{\text{con}}) := g_i(\mathbf{w}_i) + \frac{\rho\gamma_i}{2}\|\mathbf{w}_i - \mathbf{w}_{\text{con}}\|_2^2$, the sub-problem of \mathcal{C}_i becomes²

$$\begin{aligned} \mathbf{w}_i^{(t+1)} &= \underset{\mathbf{w}_i \in \mathcal{W}}{\text{argmin}} f_i(\mathbf{w}_i, \mathbf{w}_{\text{con}}^{(t)}) \\ &= \underset{\mathbf{w}_i \in \mathcal{W}}{\text{argmin}} \frac{1}{N_i} \sum_{n=1}^{N_i} \mathbf{z}_{i,n}^\top \mathbf{w}_i - \alpha \mathbf{1}^\top \log(\mathbf{S}\mathbf{w}_i + \zeta \mathbf{1}) \\ &\quad + 2\beta\|\mathbf{w}_i\|_2^2 + \frac{\rho\gamma_i}{2}\|\mathbf{w}_i - \mathbf{w}_{\text{con}}^{(t)}\|_2^2. \end{aligned} \quad (9)$$

We use the accelerated projected gradient descent algorithm to update \mathbf{w}_i . At the beginning of local updates, \mathcal{C}_i first initializes $\mathbf{w}_i^{(t,0)} = \mathbf{w}_i^{(t-1, K_i^{(t-1)})}$ and $\mathbf{w}_i^{(t,-1)} = \mathbf{w}_i^{(t-1, K_i^{(t-1)}-1)}$, where $K_i^{(t)}$ is the number of local loops of \mathcal{C}_i in the t -th outer iteration. Besides, $\mathbf{w}_i^{(t,k)}$ represents the updated graph of \mathcal{C}_i in the t -th outer iteration and the k -th local loop. We then update the i -th local graph $K_i^{(t)}$ times by

$$\mathbf{w}_{i,\text{ex}}^{(t,k)} = \mathbf{w}_i^{(t,k)} + \xi \left(\mathbf{w}_i^{(t,k)} - \mathbf{w}_i^{(t,k-1)} \right) \quad (10)$$

$$\check{\mathbf{w}}_i^{(t,k+1)} = \mathbf{w}_{i,\text{ex}}^{(t,k)} - \eta_w \left(\nabla g_i(\mathbf{w}_{i,\text{ex}}^{(t,k)}) + \rho\gamma_i^{(t)} \left(\mathbf{w}_{i,\text{ex}}^{(t,k)} - \mathbf{w}_{\text{con}}^{(t)} \right) \right) \quad (11)$$

$$\mathbf{w}_i^{(t,k+1)} = \text{Proj}_{\mathcal{W}} \left(\check{\mathbf{w}}_i^{(t,k+1)} \right), \quad (12)$$

where $\xi \in [0, 1]$ is the momentum weight. In (11), $\nabla g_i(\mathbf{w})$ is calculated as $\frac{1}{N_i} \sum_{n=1}^{N_i} \mathbf{z}_{i,n} - \alpha \mathbf{S}^\top \left(\frac{1}{\mathbf{S}\mathbf{w} + \zeta \mathbf{1}} \right) + 4\beta\mathbf{w}$. Moreover, η_w is the stepsize, the choice of which will be discussed in the next subsection. The operator $\text{Proj}_{\mathcal{W}}(\cdot)$ means projecting variables into \mathcal{W} . When local updates finish, \mathcal{C}_i sends $\mathbf{w}_i^{(t+1)}$ to the central server. Note that the local update of \mathbf{w}_i is inexact in one communication round since we run (10)-(12) for $K_i^{(t)}$ times without convergence. The reason we use inexact updates is that we are desired to update all local graphs synchronously. Due to system heterogeneity, the time required for each client to update \mathbf{w}_i until convergence may vary widely. It takes longer if the central server waits for all clients to update their graphs until convergence.

Updating \mathbf{w}_{con} and γ in the central server: The update corresponds to lines 10-12 in Algorithm 1. After the central server receives all the updated local graphs, we update $\mathbf{w}_{\text{con}}^{(t+1)}$ by solving the following problem

$$\begin{aligned} \mathbf{w}_{\text{con}}^{(t+1)} &= \underset{\mathbf{w}_{\text{con}}}{\text{argmin}} \sum_{i=1}^I f_i(\mathbf{w}_i^{(t+1)}, \mathbf{w}_{\text{con}}) + \lambda \|\mathbf{w}_{\text{con}}\|_1 \\ &= \underset{\mathbf{w}_{\text{con}}}{\text{argmin}} \sum_{i=1}^I \frac{\rho\gamma_i^{(t)}}{2} \|\mathbf{w}_i^{(t+1)} - \mathbf{w}_{\text{con}}\|_2^2 + \lambda \|\mathbf{w}_{\text{con}}\|_1. \end{aligned} \quad (13)$$

The problem is rephrased as

$$\begin{aligned} \mathbf{w}_{\text{con}}^{(t+1)} &= \underset{\mathbf{w}_{\text{con}}}{\text{argmin}} \frac{1}{2} \left\| \mathbf{w}_{\text{con}} - \frac{\sum_{i=1}^I \gamma_i^{(t)} \mathbf{w}_i^{(t+1)}}{\sum_{i=1}^I \gamma_i^{(t)}} \right\|_2^2 \\ &\quad + \frac{\lambda}{\rho \sum_{i=1}^I \gamma_i^{(t)}} \|\mathbf{w}_{\text{con}}\|_1. \end{aligned} \quad (14)$$

²In the sequel, $f_i(\mathbf{w}_i, \mathbf{w}_{\text{con}}^{(t)})$ is the function of variable \mathbf{w}_i with fixed $\mathbf{w}_{\text{con}}^{(t)}$, $f_i(\mathbf{w}_i^{(t)}, \mathbf{w}_{\text{con}})$ is the function of variable \mathbf{w}_{con} with fixed $\mathbf{w}_i^{(t)}$, and $f_i(\mathbf{w}_i, \mathbf{w}_{\text{con}})$ is the function of both \mathbf{w}_i and \mathbf{w}_{con} .

By defining $C_\gamma^{(t)} = \sum_{i=1}^I \gamma_i^{(t)}$ and $\mu^{(t)} = \frac{\lambda}{C_\gamma^{(t)} \rho}$, we obtain

$$\mathbf{w}_{\text{con}}^{(t+1)} = \text{prox}_{\mu^{(t)} \|\cdot\|_1} \left(\frac{\sum_{i=1}^I \gamma_i^{(t)} \mathbf{w}_i^{(t+1)}}{C_\gamma^{(t)}} \right), \quad (15)$$

where $\text{prox}_{\mu^{(t)} \|\cdot\|_1}(\cdot)$ is the proximal operator of ℓ_1 norm. It is observed from (15) that $\mathbf{w}_{\text{con}}^{(t+1)} \in \mathcal{W}$ since it is a combination of $\mathbf{w}_i^{(t+1)}$ with positive weights, and the proximal operator will not move the vector out of \mathcal{W} .

After obtaining $\mathbf{w}_{\text{con}}^{(t+1)}$, we adjust $\gamma_i^{(t+1)}$ using the inverse distance weighting schema [37]

$$\gamma_i^{(t+1)} = \frac{1}{2 \left\| \mathbf{w}_i^{(t+1)} - \mathbf{w}_{\text{con}}^{(t+1)} \right\|_2 + \epsilon_\gamma}, \text{ for } i = 1, \dots, I, \quad (16)$$

where ϵ_γ is a small enough constant. We place the derivation of (16) in the supplementary materials for completeness. The merit of adopting this schema is that we can automatically adjust the weight γ_i according to the difference between \mathbf{w}_i and \mathbf{w}_{con} . For the \mathbf{w}_i close to \mathbf{w}_{con} , a larger γ_i is assigned to the corresponding term, increasing the contribution of the i -th local graph to the consensus graph. Finally, we send $\mathbf{w}_{\text{con}}^{(t+1)}$ and $\gamma_i^{(t+1)}$ back to the \mathcal{C}_i .

Some discussions: Our algorithm differs from existing FL(PFL) algorithms in the following ways. (i) Unlike the algorithms of cross-device FL [14], [27], our algorithm learns graphs in a cross-silo FL scenario. Specifically, all clients, rather than a subset of clients, participate in local updates in each communication round. In addition, local clients utilize all stored data to update graphs instead of sampling a batch of data like cross-device FL algorithms [14], [27]. (ii) Our algorithm differs from existing multi-task PFL algorithms [17], [27], [29] because the optimization problems corresponding to local and global updates are customized. For example, our algorithm updates the consensus graph by solving a ℓ_1 norm regularized quadratic optimization problem, whereas the global update of existing algorithms is the aggregation of local models. (iii) Finally, compared to decentralized PFL algorithms [28], [30], our algorithm follows the ‘‘central server-clients’’ schema.

C. Convergence Analysis

In this section, we provide the convergence analysis of our algorithm. First, let us make some technical assumptions.

Assumption 1. All observed data are bounded, i.e., there exists a constant $B_z > 0$ such that $\|\mathbf{z}_{i,n}\|_2 \leq B_z$ for all $n = 1, \dots, N_i$ and $i = 1, \dots, I$.

Assumption 2. The updated graphs in the search space are bounded, i.e., for any updated \mathbf{y} and $\mathbf{y}' \in \mathcal{W}$, $\|\mathbf{y} - \mathbf{y}'\|_2 \leq B_r$. Furthermore, for any updated \mathbf{y} and $\mathbf{y}' \in \mathcal{W}$, $\|\mathbf{y} - \mathbf{y}'\|_2 \leq B_w$, where $\mathcal{W} = \text{conv}[\cup_{0 \leq \xi \leq 1} \{\mathbf{y} + \xi(\mathbf{y} - \mathbf{y}')\} \mid \mathbf{y}, \mathbf{y}' \in \mathcal{W}]$ is the feasible set extended by the momentum update.

Without loss of generality, Assumption 1 holds naturally in real-world applications. Assumption 2 holds since meaningful graphs should have finite edge weights. Furthermore, Assumption 2 indicates that the updated weights $\gamma_i^{(t)}$ via (16) are bounded in $\left[\frac{1}{2B_r + \epsilon_\gamma}, \frac{1}{\epsilon_\gamma} \right]$. The boundary is usually not reached, and hence we define two positive constants γ_{\min} and γ_{\max} to represent the possible minimum and maximum values

Algorithm 1 Privacy-preserving algorithm for solving (8)

Input: $\alpha, \beta, \rho, \xi, \lambda$, and signals $\mathbf{X}_1, \dots, \mathbf{X}_I$

- 1: **Initialize** $\gamma_i^{(0)} = 1/I$, $\mathbf{w}_{\text{con}}^{(0)} = \mathbf{w}_i^{(0)} = \mathbf{w}_i^{(-1,0)} = \mathbf{w}_i^{(-1,-1)}$ for $i = 1, \dots, I$, and let $K_i^{(-1)} = 0$
- 2: **for** $t = 0, \dots, T-1$ **do**
- 3: *// Update $\mathbf{w}_1, \dots, \mathbf{w}_I$ in parallel in local clients*
- 4: **for** $i = 1, \dots, I$ **in parallel do**
- 5: Receive $\gamma_i^{(t)}$ and $\mathbf{w}_{\text{con}}^{(t)}$ from the central server
- 6: Initialize $\mathbf{w}_i^{(t,0)} = \mathbf{w}_i^{(t-1, K_i^{(t-1)})}$ and $\mathbf{w}_i^{(t,-1)} = \mathbf{w}_i^{(t-1, K_i^{(t-1)}-1)}$
- 7: **for** $k = 0, \dots, K_i^{(t)} - 1$ **do**
- 8: Update $\mathbf{w}_i^{(t,k+1)}$ using (10)-(12)
- 9: **end for**
- 10: Let $\mathbf{w}_i^{(t+1)} = \mathbf{w}_i^{(t, K_i^{(t)})}$ and send it to central server
- 11: **end for**
- 12: *// Update \mathbf{w}_{con} and γ in central server*
- 13: Update $\mathbf{w}_{\text{con}}^{(t+1)}$ using (15)
- 14: Update $\gamma_i^{(t+1)}$ using (16), for $i = 1, \dots, I$
- 15: Send $\mathbf{w}_{\text{con}}^{(t+1)}$ and $\gamma_i^{(t+1)}$ to the i -th client \mathcal{C}_i
- 16: **end for**
- 17: **return** $\mathbf{w}_1^{(T)}, \dots, \mathbf{w}_I^{(T)}$ and $\mathbf{w}_{\text{con}}^{(T)}$

of $\gamma_i^{(t)}$ for all i and t . We have the following proposition based on Assumptions 1-2.

Proposition 1. *Under Assumptions 1-2, the objective function $f_i(\mathbf{w}_i^{(t+1)}, \mathbf{w}_{\text{con}})$ is $\rho\gamma_i^{(t)}$ -Lipschitz smooth w.r.t. \mathbf{w}_{con} , and the function $f_i(\mathbf{w}_i, \mathbf{w}_{\text{con}}^{(t)})$ is $L_i^{(t)}$ -Lipschitz smooth w.r.t. \mathbf{w}_i on $\tilde{\mathcal{W}}$, where $L_i^{(t)} := 4\beta + 2\alpha(d-1)/\zeta^2 + \rho\gamma_i^{(t)}$. Besides, the gradient of $f_i(\mathbf{w}_i, \mathbf{w}_{\text{con}}^{(t)})$ is bounded by a constant $B_f := B_z + (4\beta + \rho\gamma_{\max})B_w + \alpha\sqrt{2(d-1)}/\zeta$ for all i and t .*

Proof: We place the proof in Appendix A. ■

We further make the following assumption to determine the stepsize in Algorithm 1.

Assumption 3. *The (constant) stepsize satisfies $\eta_w \leq 1/L_{\max}$, where L_{\max} is the maximum value of $L_i^{(t)}$ for all i and t , i.e., $L_{\max} = 4\beta + 2\alpha(d-1)/\zeta^2 + \rho\gamma_{\max}$.*

This assumption is necessary for gradient descent-type algorithms. Finally, we provide the convergence analysis of our proposed algorithm as follows.

Theorem 1. *Suppose that Assumptions 1-3 hold, the sequences $\mathbf{w}_i^{(t)}$, $\mathbf{w}_{\text{con}}^{(t)}$ generated from our algorithm satisfy*

$$\frac{1}{T} \sum_{t=0}^{T-1} \left(\sum_{i=1}^I \|\mathbf{w}_i^{(t+1)} - \mathbf{w}_i^{(t)}\|_2^2 \right) \leq \frac{C_1}{T}, \quad (17)$$

$$\frac{1}{T} \sum_{t=0}^{T-1} \|\mathbf{w}_{\text{con}}^{(t+1)} - \mathbf{w}_{\text{con}}^{(t)}\|_2^2 \leq \frac{C_2}{T}, \quad (18)$$

where

$$C_1 = \frac{2\Delta\eta_w}{1-\xi^2}, \quad C_2 = \frac{2\Delta}{\rho I \gamma_{\min}},$$

$$\Delta = \sum_{i=1}^I f_i(\mathbf{w}_i^{(0)}, \mathbf{w}_{\text{con}}^{(0)}) - f_i^* + \lambda\sqrt{p}B_r. \quad (19)$$

In (19), f_i^* denotes the minimum value for $f_i(\mathbf{w}_i, \mathbf{w}_{\text{con}})$.

Proof: See Appendix B for more details. ■

The theorem reveals that as T increases, the average cumulative error between two consecutive iterations will decay to zero for both \mathbf{w}_i and \mathbf{w}_{con} , indicating that our algorithm enjoys a convergence rate of $\mathcal{O}(1/T)$.

D. Privacy analysis

In our algorithm, all data are processed locally, and local clients upload model updates instead of raw data to the central server, which protects data privacy to some extent. However, inference attacks [32] and model inversion attacks [31] show that the updates sent by local clients may still reveal users' private information. A popular technique to prevent privacy leakage when transferring model updates is DP, which provides rigorous privacy guarantees to participants. We will introduce DP into our framework in the next section.

IV. PRIVACY-PRESERVING GRAPH LEARNING WITH DIFFERENTIAL PRIVACY

A. Privacy Model

We assume the existence of an adversary who can observe the transmitted updates during the execution of the algorithm. Our goal is to prevent the eavesdroppers from learning much information about any individual data point of any local dataset from the transmitted data. To this end, we introduce DP into Algorithm 1. First, let us provide the definition of DP.

Definition 2. *((ϵ, δ)-DP [39]): For $\epsilon > 0, \delta \geq 0$, a randomized mechanism $\mathcal{M} : \mathcal{X} \rightarrow \mathcal{R}$ with domain \mathcal{X} (e.g., possible datasets) and range \mathcal{R} (e.g., possible output models) satisfies (ϵ, δ)-DP if for any two adjacent datasets $\mathcal{D}, \mathcal{D}' \in \mathcal{X}$, denoted as $\mathcal{D} \approx \mathcal{D}'$, and any subset of outputs $\mathcal{S} \subseteq \mathcal{R}$, it holds that*

$$\Pr[\mathcal{M}(\mathcal{D}) \in \mathcal{S}] \leq e^\epsilon \Pr[\mathcal{M}(\mathcal{D}') \in \mathcal{S}] + \delta. \quad (20)$$

In the definition, two datasets \mathcal{D} and \mathcal{D}' being adjacent means that they only differ in a single data point [40]. \mathcal{M} is a randomized mechanism (e.g., the Gaussian mechanism introduced below) that inputs a dataset and implements some functionality. The probability $\Pr(\cdot)$ is over the randomness of the mechanism. The parameter δ is a relaxation constant, and ϵ is called the privacy budget controlling the level of privacy guarantee achieved by \mathcal{M} [40]. By the definition, for an arbitrarily given δ , a mechanism with small ϵ guarantees that a single data point does not significantly change the output [40]. Therefore, at a high level, (20) can be interpreted as ensuring that $\mathcal{M}(\mathcal{D})$ does not reveal too much information about any single data point contained in \mathcal{D} . Applied to our model, the core problem becomes that given privacy budget (ϵ, δ) , how to design \mathcal{M}_i such that $\mathcal{M}_i(\mathcal{D}_i)$ satisfies (ϵ, δ) -DP for $i = 1, \dots, I$, where \mathcal{D}_i is the dataset of \mathcal{C}_i .

B. Algorithm

A common approach to realize DP is to add noise to the released data, which can mask the contribution of any individual data record [39]. In this study, we employ the Gaussian mechanism [13], which has applications in many fields, such as [41]. Applied to our problem, the mechanism is expressed as $\mathcal{M}(\mathcal{D}) = \varphi(\mathcal{D}) + \mathbf{s}$, where $\varphi : \mathcal{D} \rightarrow \mathbb{R}^p$ is a function generating local graphs. The Gaussian noise

$\mathbf{s} \sim \mathcal{N}^p(0, \sigma^2) \in \mathbb{R}^p$ means that each dimension of \mathbf{s} are independently from the Gaussian distribution $\mathcal{N}(0, \sigma^2)$. Specifically, we add the Gaussian noise to the gradient of (11) before local clients publish model updates. The proposed algorithm with DP is built on Algorithm 1 with some modifications for local updates, which will be explained below.

Updating \mathbf{w}_i in the local client \mathcal{C}_i : In the t -th communication round, we first perform the update of line 7 in Algorithm 1 $K_i^{(t)} - 1$ times. In the $K_i^{(t)}$ -th iteration, we add Gaussian noise to the gradient information, i.e.,

$$\mathbf{w}_{i,\text{ex}}^{(t, K_i^{(t)}-1)} = \mathbf{w}_i^{(t, K_i^{(t)}-1)} + \xi \left(\mathbf{w}_i^{(t, K_i^{(t)}-1)} - \mathbf{w}_i^{(t, K_i^{(t)}-2)} \right) \quad (21)$$

$$\begin{aligned} \tilde{\mathbf{w}}_i^{(t, K_i^{(t)})} &= \mathbf{w}_{i,\text{ex}}^{(t, K_i^{(t)}-1)} - \eta_w \left(\nabla g_i \left(\mathbf{w}_{i,\text{ex}}^{(t, K_i^{(t)}-1)} \right) \right) + \mathbf{s}_i^{(t)} \\ &\quad + \rho \gamma_i^{(t)} \left(\mathbf{w}_{i,\text{ex}}^{(t, K_i^{(t)}-1)} - \mathbf{w}_{\text{con}}^{(t)} \right) \end{aligned} \quad (22)$$

$$\mathbf{w}_i^{(t, K_i^{(t)})} = \text{Proj}_{\mathcal{W}} \left(\tilde{\mathbf{w}}_i^{(t, K_i^{(t)})} \right), \quad (23)$$

where $\mathbf{s}_i^{(t)} \sim \mathcal{N}^p \left(0, \left(\sigma_i^{(t)} \right)^2 \right)$ is the added Gaussian noise in the t -th communication round. We then set $\mathbf{w}_i^{(t+1)} = \mathbf{w}_i^{(t, K_i^{(t)})}$ and send $\mathbf{w}_i^{(t+1)}$ to the central server.

Updating \mathbf{w}_{con} and γ in the central server: The update in the central server is the same as Algorithm 1.

A central task of our algorithm is to determine the noise scale $\sigma_i^{(t)}$, which is provided in the following theorem.

Theorem 2. For $\epsilon_i^{(t)} > 0$, $\delta_i^{(t)} \in (0, 1]$, let $\sigma_i^{(t)} \geq \frac{2\sqrt{2 \ln(1.25/\delta_i^{(t)})} B_f C_s}{\epsilon_i^{(t)}}$, where

$$\begin{aligned} C_s &= \left(\frac{ra - a^2 - b}{(s+r)(1+s)} \left(1 - (-s)^{K_i^{(t)}-1} \right) \right. \\ &\quad \left. + \frac{sa + a^2 + b}{(s+r)(1-r)} \left(1 - r^{K_i^{(t)}-1} \right) + 1 \right), \\ a &= (1+\xi)(1 - \eta_w \rho \gamma_i^{(t)}), \quad b = \xi(1 - \eta_w \rho \gamma_i^{(t)}), \\ s &= \frac{-a - \sqrt{a^2 + 4b}}{2}, \quad r = \frac{a - \sqrt{a^2 + 4b}}{2}. \end{aligned} \quad (24)$$

For the noise $\mathbf{s}_i^{(t)}$ drawn from Gaussian distribution $\mathcal{N}^p \left(0, \left(\sigma_i^{(t)} \right)^2 \right)$, the mechanism $\mathcal{M}_i(\mathcal{D}_i)$ of one upload is $(\epsilon_i^{(t)}, \delta_i^{(t)})$ -DP. Furthermore, for the whole T communication rounds, the algorithm satisfies $\left(\sum_{t=0}^{T-1} \epsilon_i^{(t)}, \sum_{t=0}^{T-1} \delta_i^{(t)} \right)$ -DP.

Proof: The overall idea of this proof is to calculate the sensitivity, i.e., $\max_{\mathcal{D}_i \approx \mathcal{D}_i'} \left\| \mathbf{w}_i^{(t+1)} - \mathbf{u}_i^{(t+1)} \right\|_2$ of local updates, where $\mathbf{w}_i^{(t+1)}$ and $\mathbf{u}_i^{(t+1)}$ are local outputs based on \mathcal{D}_i and \mathcal{D}_i' , respectively. With the sensitivity, we can use the results of [40] to obtain the required noise for the Gaussian mechanism. See Appendix C for details. ■

The theorem determines the noise scale that needs to be added for a given privacy level $(\epsilon_i^{(t)}, \delta_i^{(t)})$. Compared to the algorithms in [28], [42], Theorem 2 suggests a weight

C_s on the noise scale due to multiple local updates. Usually, $\eta_w \rho \gamma_i^{(t)} \ll 1$, making a and b determined by ξ , i.e., $a \approx 1 + \xi$, $b \approx \xi$. Thus, as $K_i^{(t)}$ increases, C_s is dominated by its first term since $s \leq -a \leq -1$. More local update iterations (larger $K_i^{(t)}$) mean that more noise needs to be added for a given privacy budget. However, if $K_i^{(t)}$ is small, our algorithm requires more converging communication rounds. Consequently, for a given total privacy budget of T rounds, the privacy budget allocated to each round $(\epsilon_i^{(t)}, \delta_i^{(t)})$ will be less. Indeed, the added noise in Theorem 2 is overly large due to C_s . To reduce the noise added in each communication round, we provide the following corollary.

Corollary 1. When $K_i^{(t)} = 1$, for $\epsilon_i^{(t)} > 0$, $\delta_i^{(t)} \in (0, 1]$, the mechanism $\mathcal{M}_i(\mathcal{D}_i)$ of one communication is $(\epsilon_i^{(t)}, \delta_i^{(t)})$ -DP if the added noise $\mathbf{s}_i^{(t)} \sim \mathcal{N}^p \left(0, \left(\sigma_i^{(t)} \right)^2 \right)$, where $\sigma_i^{(t)} \geq \frac{2\sqrt{2 \ln(1.25/\delta_i^{(t)})} B_z}{\epsilon_i^{(t)} N_i}$. Furthermore, for T communication rounds, the algorithm satisfies $\left(\sum_{t=0}^{T-1} \epsilon_i^{(t)}, \sum_{t=0}^{T-1} \delta_i^{(t)} \right)$ -DP.

Proof: See Appendix D for details. ■

The corollary provides the required noise scale for a given privacy budget in the special case $K_i^{(t)} = 1$. The weight C_s caused by multiple local updates is 1 when $K_i^{(t)} = 1$. Moreover, we can bound the sensitivity of local updates by clipping \mathbf{z} [42]. Specifically, we clip \mathbf{z} as $\mathbf{z} / \max \left(1, \frac{\|\mathbf{z}\|_2}{C} \right)$, where C is a clipping threshold. This clipping ensures that B_z does not exceed $2C$.

Some discussions: We do not exploit the privacy amplification method [43] and the moment accountant method [42] to reduce the added noise for a given privacy budget since all data are used to update local graphs in our algorithm. Furthermore, in Theorem 2, the privacy budget for T communication rounds is set to the sum of each communication using the composition property. However, according to the strong composition theorem presented in [44], the required noise can be further reduced. Interested readers can refer to [44] for more details.

C. Convergence Analysis

We next discuss the effect of the added noise on algorithm convergence. To simplify the analysis, we assume $\sigma_i^{(t)} = \sigma$ for $i = 1, \dots, I$ and $t = 1, \dots, T$.

Theorem 3. Suppose Assumptions 1-3 hold, and the added Gaussian noise is $\mathbf{s}_i^{(t)} \sim \mathcal{N}^p(0, \sigma^2)$, the sequences $\mathbf{w}_i^{(t)}$, $\mathbf{w}_{\text{con}}^{(t)}$ generated from our algorithm with DP satisfy

$$\frac{1}{T} \sum_{t=0}^{T-1} \left(\sum_{i=1}^I \mathbb{E} \left[\left\| \mathbf{w}_i^{(t+1)} - \mathbf{w}_i^{(t)} \right\|_2^2 \right] \right) \leq \frac{C_1}{T} + \Delta_1 \quad (25)$$

$$\frac{1}{T} \sum_{t=0}^{T-1} \mathbb{E} \left[\left\| \mathbf{w}_{\text{con}}^{(t+1)} - \mathbf{w}_{\text{con}}^{(t)} \right\|_2^2 \right] \leq \frac{C_2}{T} + \Delta_2, \quad (26)$$

where the expectation is over the randomness of the added noise, and

$$\begin{aligned} \Delta_1 &= \frac{2\sqrt{\rho} \eta_w I \sigma (\xi B_r + \eta_w B_f) + 2p I \eta_w^2 \sigma^2}{1 - \xi^2}, \\ \Delta_2 &= \frac{2\sqrt{\rho} \sigma (\xi B_r + \eta_w B_f) + 2p \eta_w \sigma^2}{\rho \gamma_{\min}}. \end{aligned} \quad (27)$$

Proof: See supplementary materials for more details. ■

The results reveal that the average cumulative errors of our algorithm for both \mathbf{w}_i and \mathbf{w}_{con} consist of two terms. The first term is the same as that of Algorithm 1, which will decay to zero as the increase of T . The second term is a constant bias caused by the added noise. As expected, the bias is determined by the noise scale.

D. Privacy Analysis

Our algorithm with DP enjoys a rigorous theoretical guarantee, which further prevents privacy leakage during uploading model updates. As stated in Theorem 3, privacy preservation is achieved by adding noise, which inevitably affects the learned graphs. Thus, privacy level (ϵ, δ) is a trade-off between privacy considerations and learning performance.

V. EXPERIMENTS

In this section, we will test our proposed framework using both synthetic data and real-world data. First, some experimental setups are introduced.

A. Experimental Setups

1) *Graph generation:* We first generate Gaussian radial basis function (RBF) graphs \mathcal{G}_0 by following the method in [6]. Specifically, we generate 20 vertices whose coordinates are randomly in a unit square. Edge weights are calculated using $\exp(-\text{dist}(i, j)^2 / 2\sigma_r^2)$, where $\text{dist}(i, j)$ is the distance between vertices i and j , and $\sigma_r = 0.5$ is a kernel width parameter. We remove the edges whose weights are smaller than 0.7. Then, we keep a certain proportion—say q —of edges in \mathcal{G}_0 unchanged to form the consensus graph. Finally, we add $(1 - q)|\mathcal{E}_0|$ edges randomly to the consensus graph to form heterogeneous graphs $\mathcal{G}_1, \dots, \mathcal{G}_I$, where $|\mathcal{E}_0|$ is the number of edges in \mathcal{G}_0 . We denote $1 - q$ as the degree of heterogeneity.

2) *Signal generation:* For the i -th local graph \mathcal{G}_i , we generate N_i smooth signals from the distribution [6]

$$\mathbf{x}_{i,n} \sim \mathcal{N}(\mathbf{0}, \mathbf{L}_i^\dagger + \sigma_w^2 \mathbf{I}), \quad n = 1, \dots, N_i, \quad (28)$$

where σ_w is noise scale and \mathbf{L}_i is the Laplacian matrix of \mathcal{G}_i .

3) *Evaluation metric:* In topology inference, determining whether two vertices are connected can be regarded as a binary classification problem. Thus, we employ the following metrics to evaluate the classification results,

$$\begin{aligned} \text{Precision} &= \frac{\text{TP}}{\text{TP} + \text{FP}}, \quad \text{Recall} = \frac{\text{TP}}{\text{TP} + \text{FN}}, \\ \text{FS} &= \frac{2\text{TP}}{2\text{TP} + \text{FN} + \text{FP}}, \end{aligned} \quad (29)$$

where TP is true positive rate, TN is true negative rate, FP is the false positive rate and FN denotes false negative rate. The third metric, F1-score (FS) is the harmonic mean of Precision and Recall. The next metric is the relative error (RE)

$$\text{RE} = \frac{\|\hat{\mathbf{w}} - \mathbf{w}_{\text{gt}}\|_2}{\|\mathbf{w}_{\text{gt}}\|_2}, \quad (30)$$

where $\hat{\mathbf{w}}$ is the learned graph, and \mathbf{w}_{gt} is the groundtruth. The results of all metrics for local graphs are the average of I clients.

4) *Baselines:* We use classic FL algorithm, FedAvg [14], to solve the following problem as our baseline,

$$\min_{\mathbf{w} \in \mathcal{W}} \frac{1}{N'} \sum_{i=1}^I \sum_{n=1}^{N_i} \mathbf{z}_{i,n}^\top \mathbf{w} - \alpha \mathbf{1}^\top \log(\mathbf{S}\mathbf{w} + \zeta \mathbf{1}) + 2\beta \|\mathbf{w}\|_2^2, \quad (31)$$

where $N' = \sum_{i=1}^I N_i$. The model learns a global graph collaboratively using data from all clients regardless of data heterogeneity. We also employ a baseline called IGL (independent graph learning), where all local clients learn graphs independently using their local data. IGL enjoys full privacy as local clients do not release any data, including model updates. For our privacy-preserving algorithm, we use PPGL-L and PPGL-C to represent the learned local and consensus graphs.

5) *Determination of parameters:* For our model, α is fixed as 1, and β is selected as the value achieving the best FS in IGL. Parameters ρ and λ are determined by grid search in different cases. On algorithmic side, we set $\xi = 0.1, K_i^{(t)} = 1, T = 50$. The stepsize η_w is 0.01, which is small enough to satisfy $\eta_w \leq 1/L_{\max}$. Furthermore, we let $I = 5$ and $\sigma_w = 0.1$ for synthetic data. Some other parameters will be determined in specific experiments. All parameters of baselines are selected as those achieving the best FS values.

B. Synthetic Data

1) *Data size:* We first test the effect of data size. We fix q as 0.5 and assume all clients have the same data size, i.e., $N_i = N, i = 1, \dots, I$. We vary N from 10 to 100, and the results are shown in Table I. It is observed that FedAvg tends to obtain high Recall, meaning that the corresponding graphs contain more edges. When N increases, FedAvg yields the worst FS. The reason is that FedAvg learns a single global graph using data from all clients. However, local graphs are heterogeneous in our experiment. Therefore, the learned global graph is far from local graphs. In sharp contrast, IGL learns local graphs independently and achieves better performance than FedAvg when N is large. Our model also learns a personalized graph for each local client. Unlike IGL, we learn all local graphs jointly via a consensus graph, leading to better performance than IGL. Additionally, our model learns a consensus graph that captures the common structures of local graphs. As depicted in Fig.2, the learned graph of FedAvg has the most edges since FedAvg can hardly learn specific structures of local graphs. Our model learns both common and specific structures, while IGL fails to learn common structures.

We also test our model in the case of varying data sizes. We set N_i to 20, 40, 60, 80, and 100 for $\mathcal{C}_1 - \mathcal{C}_5$, respectively. As illustrated in Fig.3, clients with larger N_i perform better than those with small N_i . However, our model can improve the performance of clients with small N_i because they can “borrow” information from the clients with large N_i .

2) *Data heterogeneity:* We next explore the effect of data heterogeneity. In this experiment, we fix $N_i = 50$ for all clients and vary q from 0.3 to 0.9. As listed in Table II, when data heterogeneity is small (large q), FedAvg achieves satisfactory performance since the consensus graph is close to local graphs. In this case, FedAvg benefits from using all data to learn a global graph. However, as the increase of data heterogeneity, the performance of FedAvg sharply decreases. Our model

TABLE I: Performance of different data sizes.

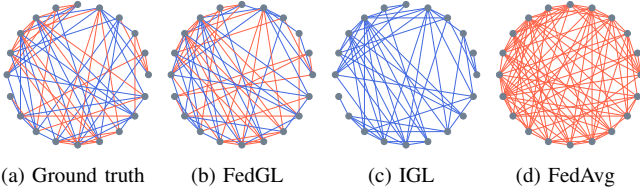
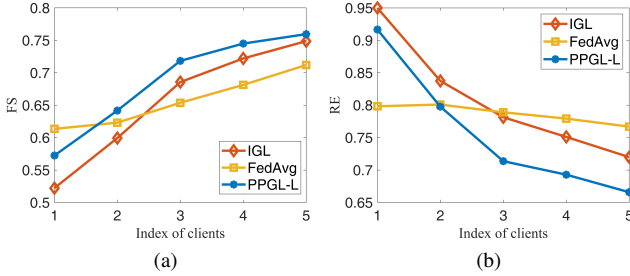
	$N = 20$				$N = 50$				$N = 100$			
	Precision	Recall	FS	RE	Precision	Recall	FS	RE	Precision	Recall	FS	RE
IGL	0.594	0.469	0.521	0.915	0.692	0.620	0.651	0.778	0.776	0.739	0.755	0.698
FedAvg	0.434	0.759	0.552	0.802	0.464	0.792	0.584	0.768	0.519	0.789	0.624	0.744
PPGL-L	0.547	0.579	0.561	0.911	0.625	0.760	0.678	0.731	0.698	0.870	0.774	0.619
PPGL-C	0.636	0.516	0.566	0.874	0.781	0.656	0.710	0.701	0.881	0.736	0.800	0.627

TABLE II: Performance of different data heterogeneity.

	$q = 0.3$				$q = 0.6$				$q = 0.9$			
	Precision	Recall	FS	RE	Precision	Recall	FS	RE	Precision	Recall	FS	RE
IGL	0.701	0.593	0.640	0.783	0.736	0.645	0.685	0.758	0.822	0.706	0.759	0.717
FedAvg	0.385	0.841	0.527	0.835	0.460	0.867	0.599	0.783	0.811	0.922	0.862	0.672
PPGL-L	0.637	0.736	0.679	0.740	0.661	0.776	0.715	0.700	0.800	0.812	0.805	0.635
PPGL-C	0.462	0.516	0.487	0.874	0.653	0.726	0.687	0.752	0.825	0.927	0.873	0.634

TABLE III: The learned γ of different clients

Index of clients	1	2	3	4	5
Data size	0.541	0.584	0.661	0.707	0.718
Graph heterogeneity	0.837	0.808	0.720	0.735	0.584

Fig. 2: The learned graphs of different methods ($N_i = 100$). In (a)-(b), red edges are those in the consensus graph, while blue edges are the edges in only in the local graphs.Fig. 3: The results of varying data sizes. The data sizes of $C_1 - C_5$ are set to 20, 40, 60, 80, and 100, respectively.

also learns a consensus graph representing global information, which shows better performance than FedAvg. On the other hand, our model suffers less from graph heterogeneity since we learn a personalized graph for each client.

3) *Adaptive weights*: Then, we test the effectiveness of the method of adjusting weights (16). Two factors are considered, i.e., data size and data heterogeneity. For data size, we let q be 0.5 and set N_i to 20, 40, 60, 80, and 100 for $C_1 - C_5$, respectively. For data heterogeneity, we fix $N_i = 100$ and first generate a graph \mathcal{G}_1 for C_1 . The graphs of $C_2 - C_5$ are generated based on \mathcal{G}_1 with q equal to 0.8, 0.6, 0.4, and 0.2, respectively. The results are displayed in Table III, and two trends can be observed. First, local graphs with large data sizes contribute more to the consensus graph. Second, local graphs close to the consensus graph obtain larger weights. Therefore, the weight adjustment strategy can effectively allocate a reasonable weight for each client.

4) *Parameter sensitivity*: In this experiment, we set $N_i =$

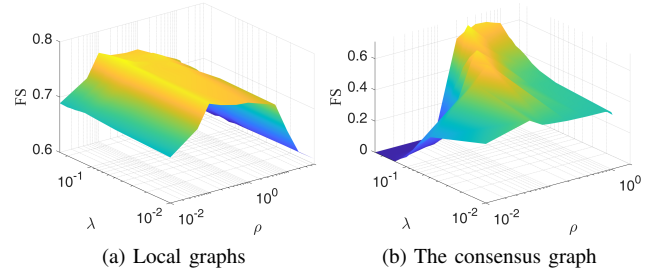


Fig. 4: The results of parameter sensitivity.

50 and $q = 0.5$, and evaluate the learning performance of different λ and ρ . As displayed in Fig.4, the performance of local graphs is hardly affected by λ . However, there exists an optimal ρ for local graphs that achieves the highest FS. On the other hand, the learned consensus graph relies on the choice of both λ and ρ . For small ρ , the FS values of consensus graphs approach zero as the increase of λ . For large ρ , the optimal λ also becomes large. We need to grid search for the optimal combination of ρ and λ , especially for consensus graphs.

5) *Differential privacy*: We also verify the effect of DP. We fix $q = 0.5$, $N_i = N$, $\bar{\delta}_i^{(t)} = \bar{\delta} = 10^{-5}$ and set equal privacy budgets for all i and t , i.e., $\bar{\epsilon}_i^{(t)} = \bar{\epsilon}$. The noise is added by following Corollary 1. We let $C = 20$, which is large enough that hardly any data needs to be clipped. We vary N and test the performance of local graphs. As listed in Table IV, our model without DP performs best. The performance of the algorithms with DP is inferior to that without DP due to the added noise. Smaller $\bar{\epsilon}$ means stronger privacy protection, and hence more noise is added, resulting in worse performance. In general, our algorithms with DP outperform IGL—a baseline with perfect privacy protection—and further guarantee a certain level of privacy protection. For small $\bar{\epsilon}$, e.g., $\bar{\epsilon} = 0.5$, our algorithm fails to obtain better performance than IGL when N is small.

TABLE IV: The results of the algorithm with DP.

	$N = 50$		$N = 100$		$N = 200$	
	FS	RE	FS	RE	FS	RE
IGL	0.646	0.782	0.725	0.701	0.808	0.595
PPGL-L	0.709	0.683	0.767	0.614	0.828	0.518
PPGL-L ($\bar{\epsilon} = 0.5$)	0.615	0.813	0.709	0.706	0.811	0.581
PPGL-L ($\bar{\epsilon} = 0.8$)	0.651	0.761	0.732	0.647	0.819	0.564
PPGL-L ($\bar{\epsilon} = 1.0$)	0.694	0.721	0.754	0.634	0.823	0.567

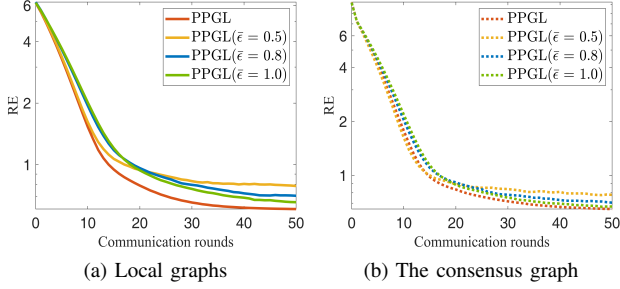


Fig. 5: The convergence of the proposed algorithm.

However, it can regain its advantage for large N since less noise is added as N increases, as suggested in Corollary 1.

6) *Convergence*: Finally, we test the convergence of the proposed algorithms. Fig.5 shows the algorithms with and without DP converge in limited communication rounds. Furthermore, algorithms with DP are biased compared to that without DP due to the added artificial noise, as illustrated in Theorem 3.

C. Real-world Data

1) *COIL-20 data*: We employ the COIL-20 dataset³, which is a collection of gray-scale images including 20 objects taken from 360 degrees, to learn the relationships between these images. Each object has 72 images (five degrees an image) of size 32×32 . We randomly select four objects and divide the images of each object into three views. Each view contains images taken in consecutive 60 degrees, e.g., $[0^\circ, 55^\circ]$. Therefore, each view contains 48 images taken from 4 objects, i.e., 12 images per object. A basic assumption is that the 48 images of different views are defined on the same node set. The image itself is taken as graph signals, i.e., $\mathbf{X}_i \in \mathbb{R}^{48 \times 1024}$. Data distributions of different views are heterogeneous because they are from different shooting angles. Furthermore, we assume that photos from three views are taken by three different photographers, and they are reluctant to share their photos, which is the concern of this study. Our goal is to learn a graph representing the relationships among these 48 images for each view, i.e., $I = 3$, under privacy constraints. The three graphs should share some common structures because they come from the same objects. Moreover, there should be four communities in the relation graphs since all images belong to four objects. Therefore, to evaluate the learned graphs, we employ the Louvain algorithm [45] to detect communities in the learned graphs. Three metrics are leveraged to evaluate the detection results, i.e., normalized mutual information (NMI), Fowlkes and Mallows index (FMI) [46], and Rand Index (RI). The

TABLE V: The community detection results of graphs learned by different methods.

	IGL	FedAvg	PPGL-C Non-DP	PPGL-C $\bar{\epsilon} = 0.5$	PPGL-C $\bar{\epsilon} = 0.8$	PPGL-C $\bar{\epsilon} = 1.0$
NMI	0.851	0.857	1	1	1	1
RI	0.879	0.872	1	1	1	1
FMI	0.801	0.842	1	1	1	1

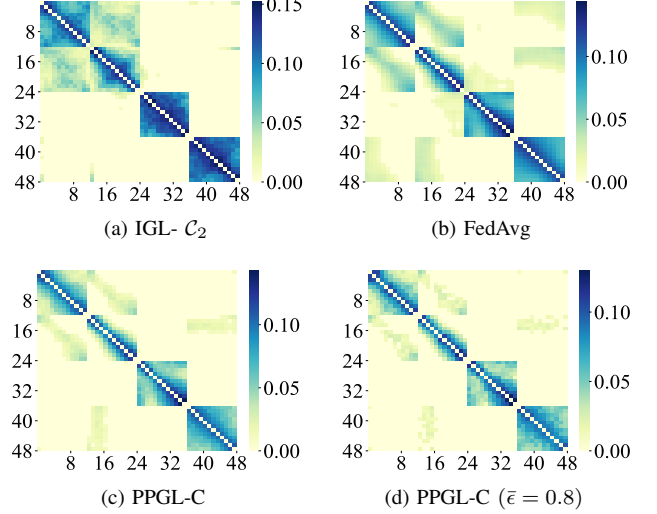


Fig. 6: The learned graphs with different methods.

labels of images are taken as the ground-truth. The detection results of our model are based on consensus graphs, while the results related to IGL are the average of three local views. As displayed in Table V, the Louvain algorithm successfully finds all communities in the graphs learned by our models. Instead, some mistakes are made in the graphs learned by IGL and FedAvg. This is expected since the consensus graph captures the common structure of local graphs, which may remove noisy edges of different views. Finally, despite adding random noise to the uploaded data, our models with DP guarantee still show satisfactory detection results. As shown in Fig.6, the communities can be observed in the consensus graphs. However, more confusing edges appear in the graphs of IGL and FedAvg.

2) *Medical data*: We finally employ blood-oxygenation-level-dependent (BOLD) time series extracted from fMRI data to learn brain functional connectivity graphs. The basic assumption is that autism may affect brain functional connectivity. If we can learn about the differences in brain functional connectivity graphs between autistic and non-autistic people, it may help us better understand the mechanism of autism. However, medical data are privacy-sensitive, and their transmission to an unreliable central server is usually prohibited. In this experiment, the used dataset⁴ contains 539 autistic individuals and 573 typical controls, from which we select three autistic and three non-autistic subjects. Each client (subject) contains 176 signals (the length of BOLD time series is 176), which are divided into 150 training data and 26 testing

³<https://www.cs.columbia.edu/CAVE/software/softlib/coil-20.php>

⁴<http://preprocessed-connectomes-project.org/abide/>

TABLE VI: The reconstruction performance using graphs learned by different models

	IGL	FedAvg	PPGL-L	PPGL-L	PPGL-L
				$\epsilon = 0.8$	$\epsilon = 1$
RE	0.778	0.796	0.741	0.771	0.762

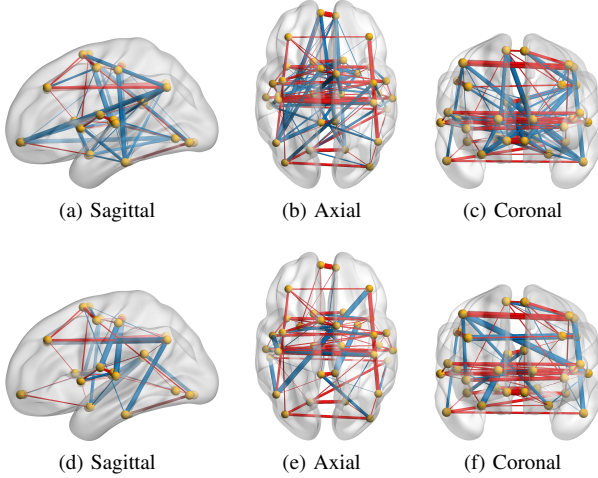


Fig. 7: The figure depicts our learned graphs (without DP) from three views. The top and bottom rows show the graphs of non-autistic and autistic subjects, respectively. The red edges are those in the consensus graph, while the blue edges are those specific edges in local graphs.

data. Besides, we select 34 functional regions of interest from 90 standard regions of the Anatomical Automatic Labeling (AAL) template, indicating that $\mathbf{X}_i \in \mathbb{R}^{34 \times 150}$, $i = 1, \dots, 6$. To evaluate the learned graphs, we mask some nodes of the testing graphs signals and use the signals of the observed nodes to reconstruct those of the masked nodes via the learned graphs [47]. The evaluation metric is the relative error between the reconstructed signals and the ground-truth. If the learned graph better reflects the underlying topology behind data, the reconstructed signals should be close to the real signals. As listed in Table VI, our model achieves the best reconstruction performance, meaning that our model can learn a graph better reflecting the topological relationship of data, even those with DP guarantees. Figure 7 depicts the learned graphs using our model. It is observed that graphs of autistic and non-autistic individuals share many common edges that are learned in the consensus graph. On the other hand, there are some noticeable topological changes between the graphs of autistic and non-autistic individuals. These edges reflect changes in the functional connectivity caused by autism, which may aid in diagnosing autism. Furthermore, the graphs of autistic individuals display fewer edges, which is consistent with the current study [48]. In the future, a domain expert may help interpret the results from a medical perspective.

VI. CONCLUSION

In this paper, we proposed a framework to learn graphs under privacy constraints. In our framework, multiple personalized graphs and a consensus graph were jointly learned to handle data heterogeneity. Then, we devised a privacy-preserving

algorithm, in which all private data are processed in local clients. To further enhance privacy preservation, we introduced DP into our framework to resist privacy attacks when transmitting model updates. Convergence analyses for the proposed algorithms were provided, including that with DP. Extensive experiments showed that our approach can efficiently learn graphs under privacy constraints. Future research may include generalizing our framework to other graph learning models except for the smoothness assumption.

APPENDIX A PROOF OF PROPOSITION 1

The proof is mainly from [49] but with some modifications.

For two vectors \mathbf{y} and \mathbf{y}' in \mathcal{W} , we have that

$$\begin{aligned}
 & \left\| \nabla_{\mathbf{y}} f_i(\mathbf{y}, \mathbf{w}_{\text{con}}^{(t)}) - \nabla_{\mathbf{y}'} f_i(\mathbf{y}', \mathbf{w}_{\text{con}}^{(t)}) \right\|_2 \\
 &= \left\| 4\beta(\mathbf{y} - \mathbf{y}') - \alpha \mathbf{S}^\top \left(\frac{1}{\mathbf{S}\mathbf{y} + \zeta \mathbf{1}} - \frac{1}{\mathbf{S}\mathbf{y}' + \zeta \mathbf{1}} \right) + \rho \gamma_i^{(t)}(\mathbf{y} - \mathbf{y}') \right\|_2 \\
 &\leq 4\beta \|\mathbf{y} - \mathbf{y}'\|_2 + \alpha \|\mathbf{S}^\top\|_2 \left\| \frac{1}{\mathbf{S}\mathbf{y} + \zeta \mathbf{1}} - \frac{1}{\mathbf{S}\mathbf{y}' + \zeta \mathbf{1}} \right\|_2 + \rho \gamma_i^{(t)} \|\mathbf{y} - \mathbf{y}'\|_2 \\
 &\leq 4\beta \|\mathbf{y} - \mathbf{y}'\|_2 + \frac{\alpha \|\mathbf{S}\|_2}{\zeta^2} \|\mathbf{S}\mathbf{y} - \mathbf{S}\mathbf{y}'\|_2 + \rho \gamma_i^{(t)} \|\mathbf{y} - \mathbf{y}'\|_2 \\
 &\leq 4\beta \|\mathbf{y} - \mathbf{y}'\|_2 + \frac{\alpha \|\mathbf{S}\|_2^2}{\zeta^2} \|\mathbf{y} - \mathbf{y}'\|_2 + \rho \gamma_i^{(t)} \|\mathbf{y} - \mathbf{y}'\|_2 \\
 &= \left(4\beta + \frac{2\alpha(d-1)}{\zeta^2} + \rho \gamma_i^{(t)} \right) \|\mathbf{y} - \mathbf{y}'\|_2 \triangleq L_i^{(t)} \|\mathbf{y} - \mathbf{y}'\|_2,
 \end{aligned} \tag{32}$$

The first inequality holds due to the triangle inequality, while the last equality holds due to Assumption 1-2 and Lemma 1 in [49]. From (32), we can conclude that f_i is $L_i^{(t)}$ -Lipschitz smooth w.r.t. \mathbf{w}_i on \mathcal{W} . On the other hand, we obtain that

$$\left\| \nabla_{\mathbf{y}} f_i(\mathbf{w}_i^{(t+1)}, \mathbf{y}) - \nabla_{\mathbf{y}'} f_i(\mathbf{w}_i^{(t+1)}, \mathbf{y}') \right\|_2 = \rho \gamma_i^{(t)} \|\mathbf{y} - \mathbf{y}'\|_2 \tag{33}$$

Therefore, f_i is $\rho \gamma_i^{(t)}$ -Lipschitz smooth w.r.t. \mathbf{w}_{con} . The last part of the proof is to calculate the bound of the gradient $\nabla_{\mathbf{w}_i} f_i(\mathbf{w}_i, \mathbf{w}_{\text{con}}^{(t)})$ for $\mathbf{w}_i \in \mathcal{W}$, i.e.,

$$\begin{aligned}
 & \left\| \nabla_{\mathbf{w}_i} f_i(\mathbf{w}_i, \mathbf{w}_{\text{con}}^{(t)}) \right\|_2 \\
 &= \left\| \frac{1}{N_i} \sum_n \mathbf{z}_{i,n} + 4\beta \mathbf{w}_i - \alpha \mathbf{S}^\top \left(\frac{1}{\mathbf{S}\mathbf{w}_i + \zeta \mathbf{1}} \right) + \rho \gamma_i^{(t)} (\mathbf{w}_i - \mathbf{w}_{\text{con}}^{(t)}) \right\|_2 \\
 &\leq \frac{1}{N_i} \sum_n \|\mathbf{z}_{i,n}\|_2 + 4\beta \|\mathbf{w}_i\|_2 + \alpha \|\mathbf{S}\|_2 \left\| \frac{1}{\mathbf{S}\mathbf{w}_i + \zeta \mathbf{1}} \right\|_2 \\
 &\quad + \rho \gamma_i^{(t)} \|\mathbf{w}_i - \mathbf{w}_{\text{con}}^{(t)}\|_2 \\
 &\leq B_z + (4\beta + \rho \gamma_i^{(t)}) B_w + \alpha \sqrt{2(d-1)}/\zeta \\
 &\leq B_z + (4\beta + \rho \gamma_{\max}) B_w + \alpha \sqrt{2(d-1)}/\zeta \triangleq B_f,
 \end{aligned} \tag{34}$$

where the second inequality holds due to Assumptions 1-2 and Lemma 1 in [49]. The last inequality holds since $\gamma_{\max} \geq \gamma_i^{(t)}$.

APPENDIX B PROOF OF THEOREM 1

For notational simplicity, we fix $K_i^{(t)} = 1$ and omit the epoch index k in local clients (only one epoch of update is

performed in local clients). We remark that the proof can be easily extended to general cases where $K_i^{(t)} > 1$. Before we start the proof, some lemmas are provided.

Lemma 1. Suppose that Assumptions 1-3 hold, for any client C_i , the updated $\mathbf{w}_i^{(t+1)}$ satisfies that

$$f_i(\mathbf{w}_i^{(t+1)}, \mathbf{w}_{\text{con}}^{(t)}) \leq f_i(\mathbf{w}_i^{(t)}, \mathbf{w}_{\text{con}}^{(t)}) - \frac{1}{2\eta_w} \|\mathbf{w}_i^{(t+1)} - \mathbf{w}_i^{(t)}\|_2^2 + \frac{\xi^2}{2\eta_w} \|\mathbf{w}_i^{(t)} - \mathbf{w}_i^{(0)}\|_2^2 \quad (35)$$

Proof: Recall that $f_i(\mathbf{w}_i, \mathbf{w}_{\text{con}}^{(t)})$ is convex and $L_i^{(t)}$ -Lipschitz smooth w.r.t. \mathbf{w}_i as Proposition 1 states. Thus in the t -th iteration, given $\gamma_1^{(t)}, \dots, \gamma_I^{(t)}$, we obtain that

$$f_i(\mathbf{w}_i^{(t+1)}, \mathbf{w}_{\text{con}}^{(t)}) \leq f_i(\mathbf{w}_i^{(t)}, \mathbf{w}_{\text{con}}^{(t)}) + \frac{L_i^{(t)}}{2} \|\mathbf{w}_i^{(t+1)} - \mathbf{w}_{i,\text{ex}}^{(t)}\|_2^2 + \langle \nabla_{\mathbf{w}_i} f_i(\mathbf{w}_{i,\text{ex}}^{(t)}, \mathbf{w}_{\text{con}}^{(t)}), \mathbf{w}_i^{(t+1)} - \mathbf{w}_{i,\text{ex}}^{(t)} \rangle \quad (36)$$

$$f_i(\mathbf{w}_i^{(t)}, \mathbf{w}_{\text{con}}^{(t)}) \geq f_i(\mathbf{w}_{i,\text{ex}}^{(t)}, \mathbf{w}_{\text{con}}^{(t)}) + \langle \nabla_{\mathbf{w}_i} f_i(\mathbf{w}_{i,\text{ex}}^{(t)}, \mathbf{w}_{\text{con}}^{(t)}), \mathbf{w}_i^{(t)} - \mathbf{w}_{i,\text{ex}}^{(t)} \rangle, \quad (37)$$

where the first inequality holds because of the definition of $L_i^{(t)}$ -Lipschitz smooth, and the second inequality holds since $f_i(\mathbf{w}_i, \mathbf{w}_{\text{con}}^{(t)})$ is a convex function w.r.t \mathbf{w}_i . Combining the two inequalities, we have

$$\begin{aligned} & f_i(\mathbf{w}_i^{(t+1)}, \mathbf{w}_{\text{con}}^{(t)}) \\ & \leq f_i(\mathbf{w}_i^{(t)}, \mathbf{w}_{\text{con}}^{(t)}) + \langle \nabla_{\mathbf{w}_i} f_i(\mathbf{w}_{i,\text{ex}}^{(t)}, \mathbf{w}_{\text{con}}^{(t)}), \mathbf{w}_i^{(t+1)} - \mathbf{w}_i^{(t)} \rangle \\ & \quad + \frac{1}{2\eta_w} \|\mathbf{w}_i^{(t+1)} - \mathbf{w}_{i,\text{ex}}^{(t)}\|_2^2 \\ & \leq f_i(\mathbf{w}_i^{(t)}, \mathbf{w}_{\text{con}}^{(t)}) + \left\langle \frac{1}{\eta_w} (\mathbf{w}_i^{(t+1)} - \mathbf{w}_{i,\text{ex}}^{(t)}), \mathbf{w}_i^{(t)} - \mathbf{w}_i^{(t+1)} \right\rangle \\ & \quad + \frac{1}{2\eta_w} \|\mathbf{w}_i^{(t+1)} - \mathbf{w}_{i,\text{ex}}^{(t)}\|_2^2 \\ & \leq f_i(\mathbf{w}_i^{(t)}, \mathbf{w}_{\text{con}}^{(t)}) - \frac{1}{2\eta_w} \|\mathbf{w}_i^{(t+1)} - \mathbf{w}_i^{(t)}\|_2^2 + \frac{1}{2\eta_w} \|\mathbf{w}_i^{(t)} - \mathbf{w}_{i,\text{ex}}^{(t)}\|_2^2 \\ & = f_i(\mathbf{w}_i^{(t)}, \mathbf{w}_{\text{con}}^{(t)}) - \frac{1}{2\eta_w} \|\mathbf{w}_i^{(t+1)} - \mathbf{w}_i^{(t)}\|_2^2 \\ & \quad + \frac{\xi^2}{2\eta_w} \|\mathbf{w}_i^{(t)} - \mathbf{w}_i^{(t-1)}\|_2^2 \end{aligned} \quad (38)$$

where the first inequality holds due to $\eta_w < 1/L_{\max}$. The second inequality holds since updating $\mathbf{w}_i^{(t+1)}$ via (11) and (12) is equivalent to the following problem

$$\begin{aligned} \mathbf{w}_i^{(t+1)} = \operatorname{argmin}_{\mathbf{y} \in \mathcal{W}} & \left\langle \nabla_{\mathbf{w}_i} f_i(\mathbf{w}_{i,\text{ex}}^{(t)}, \mathbf{w}_{\text{con}}^{(t)}), \mathbf{y} \right\rangle \\ & + \frac{1}{2\eta_w} \|\mathbf{y} - \mathbf{w}_{i,\text{ex}}^{(t)}\|_2^2, \end{aligned} \quad (39)$$

which satisfies the following first-order optimality condition for any $\mathbf{y} \in \mathcal{W}$

$$\left\langle \nabla_{\mathbf{w}_i} f_i(\mathbf{w}_{i,\text{ex}}^{(t)}, \mathbf{w}_{\text{con}}^{(t)}) + \frac{1}{\eta_w} (\mathbf{w}_i^{(t+1)} - \mathbf{w}_{i,\text{ex}}^{(t)}), \mathbf{y} - \mathbf{w}_i^{(t+1)} \right\rangle \geq 0. \quad (40)$$

The third inequality of (38) holds since

$$\begin{aligned} & \left\langle \mathbf{w}_i^{(t+1)} - \mathbf{w}_{i,\text{ex}}^{(t)}, \mathbf{w}_i^{(t)} - \mathbf{w}_i^{(t+1)} \right\rangle \\ & = \frac{1}{2} \left(\|\mathbf{w}_i^{(t)} - \mathbf{w}_{i,\text{ex}}^{(t)}\|_2^2 - \|\mathbf{w}_i^{(t+1)} - \mathbf{w}_{i,\text{ex}}^{(t)}\|_2^2 - \|\mathbf{w}_i^{(t+1)} - \mathbf{w}_i^{(t)}\|_2^2 \right). \end{aligned} \quad (41)$$

Finally, we complete the proof. ■

Lemma 2. Suppose Assumptions 2-3 hold, the updated $\mathbf{w}_{\text{con}}^{(t+1)}$ satisfies that

$$\begin{aligned} & \sum_i^I f_i(\mathbf{w}_i^{(t+1)}, \mathbf{w}_{\text{con}}^{(t+1)}) + \lambda \|\mathbf{w}_{\text{con}}^{(t+1)}\|_1 \\ & \leq \sum_i^I f_i(\mathbf{w}_i^{(t+1)}, \mathbf{w}_{\text{con}}^{(t)}) + \lambda \|\mathbf{w}_{\text{con}}^{(t)}\|_1 - \frac{\rho C_\gamma^{(t)}}{2} \|\mathbf{w}_{\text{con}}^{(t+1)} - \mathbf{w}_{\text{con}}^{(t)}\|_2^2. \end{aligned} \quad (42)$$

Proof: For simplicity, we first define $F(\mathbf{w}_{\text{con}}) = \sum_i^I f_i(\mathbf{w}_i^{(t+1)}, \mathbf{w}_{\text{con}})$, and $\nabla_{\mathbf{w}_{\text{con}}} F(\mathbf{w}_{\text{con}}^{(t)})$ is simplified as $\nabla F(\mathbf{w}_{\text{con}}^{(t)})$. Since $f_i(\mathbf{w}_i^{(t+1)}, \mathbf{w}_{\text{con}})$ is $\rho\gamma_i^{(t)}$ -convex w.r.t. \mathbf{w}_{con} , $F(\mathbf{w}_{\text{con}})$ is $\rho C_\gamma^{(t)}$ -convex w.r.t. \mathbf{w}_{con} , and we obtain

$$\begin{aligned} F(\mathbf{w}_{\text{con}}^{(t+1)}) & \leq F(\mathbf{w}_{\text{con}}^{(t)}) + \langle \nabla F(\mathbf{w}_{\text{con}}^{(t)}), \mathbf{w}_{\text{con}}^{(t+1)} - \mathbf{w}_{\text{con}}^{(t)} \rangle \\ & \quad + \frac{\rho C_\gamma^{(t)}}{2} \|\mathbf{w}_{\text{con}}^{(t+1)} - \mathbf{w}_{\text{con}}^{(t)}\|_2^2. \end{aligned} \quad (43)$$

On the other hand, due to the convexity of $F(\mathbf{w}_{\text{con}}^{(t+1)})$, for any $\mathbf{y} \in \mathcal{W}$, we have $F(\mathbf{y}) \geq F(\mathbf{w}_{\text{con}}^{(t)}) + \langle \nabla F(\mathbf{w}_{\text{con}}^{(t)}), \mathbf{y} - \mathbf{w}_{\text{con}}^{(t)} \rangle$. Combining it with (43), we finally reach that

$$\begin{aligned} F(\mathbf{w}_{\text{con}}^{(t+1)}) & \leq F(\mathbf{y}) - \langle \nabla F(\mathbf{w}_{\text{con}}^{(t)}), \mathbf{w}_{\text{con}}^{(t+1)} - \mathbf{y} \rangle \\ & \quad + \frac{\rho C_\gamma^{(t)}}{2} \|\mathbf{w}_{\text{con}}^{(t+1)} - \mathbf{w}_{\text{con}}^{(t)}\|_2^2. \end{aligned} \quad (44)$$

We next focus on $h(\mathbf{w}_{\text{con}}) = \|\mathbf{w}_{\text{con}}\|_1$. Recall that $\mathbf{w}_{\text{con}}^{(t+1)} = \operatorname{prox}_{\mu^{(t)} \|\cdot\|_1} \left(\frac{\sum_{i=1}^I \gamma_i^{(t)} \mathbf{w}_i^{(t+1)}}{C_\gamma^{(t)}} \right) = \operatorname{argmin}_{\mathbf{w}_{\text{con}}} \frac{1}{2} \left\| \mathbf{w}_{\text{con}} - \frac{\sum_{i=1}^I \gamma_i^{(t)} \mathbf{w}_i^{(t+1)}}{C_\gamma^{(t)}} \right\|_2^2 + \frac{\lambda}{\rho C_\gamma^{(t)}} \|\mathbf{w}_{\text{con}}\|_1$. Define $\frac{\sum_{i=1}^I \gamma_i^{(t)} \mathbf{w}_i^{(t+1)}}{C_\gamma^{(t)}} = \mathbf{w}_{\text{avg}}^{(t+1)}$, by optimal conditions we obtain

$$\begin{aligned} 0 & \in \frac{\rho C_\gamma^{(t)}}{\lambda} (\mathbf{w}_{\text{con}}^{(t+1)} - \mathbf{w}_{\text{avg}}^{(t+1)}) + \partial h(\mathbf{w}_{\text{con}}^{(t+1)}) \\ \Rightarrow \frac{\rho C_\gamma^{(t)}}{\lambda} (\mathbf{w}_{\text{con}}^{(t+1)} - \mathbf{w}_{\text{avg}}^{(t+1)}) & \in \partial h(\mathbf{w}_{\text{con}}^{(t+1)}) \end{aligned} \quad (45)$$

Similarly, due to the convexity of $h(\mathbf{w}_{\text{con}})$, we have $h(\mathbf{y}) \geq h(\mathbf{w}_{\text{con}}^{(t+1)}) + \langle \partial h(\mathbf{w}_{\text{con}}^{(t+1)}), \mathbf{y} - \mathbf{w}_{\text{con}}^{(t+1)} \rangle$. Combining it with (44) and (45), we obtain

$$\begin{aligned} & F(\mathbf{w}_{\text{con}}^{(t+1)}) + \lambda h(\mathbf{w}_{\text{con}}^{(t+1)}) \leq F(\mathbf{y}) + \lambda h(\mathbf{y}) + \langle \nabla F(\mathbf{w}_{\text{con}}^{(t)}), \mathbf{w}_{\text{con}}^{(t+1)} - \mathbf{y} \rangle \\ & \quad + \rho C_\gamma^{(t)} (\mathbf{w}_{\text{avg}}^{(t+1)} - \mathbf{w}_{\text{con}}^{(t+1)}), \mathbf{w}_{\text{con}}^{(t+1)} - \mathbf{y} \rangle \\ & \quad + \frac{\rho C_\gamma^{(t)}}{2} \|\mathbf{w}_{\text{con}}^{(t+1)} - \mathbf{w}_{\text{con}}^{(t)}\|_2^2 \\ \Rightarrow F(\mathbf{w}_{\text{con}}^{(t+1)}) + \lambda h(\mathbf{w}_{\text{con}}^{(t+1)}) & \leq F(\mathbf{y}) + \lambda h(\mathbf{y}) \\ & \quad + \rho C_\gamma^{(t)} \langle \mathbf{w}_{\text{con}}^{(t)} - \mathbf{w}_{\text{con}}^{(t+1)}, \mathbf{w}_{\text{con}}^{(t+1)} - \mathbf{y} \rangle \\ & \quad + \frac{\rho C_\gamma^{(t)}}{2} \|\mathbf{w}_{\text{con}}^{(t+1)} - \mathbf{w}_{\text{con}}^{(t)}\|_2^2 \\ \stackrel{\mathbf{y} = \mathbf{w}_{\text{con}}^{(t)}}{\Rightarrow} F(\mathbf{w}_{\text{con}}^{(t+1)}) + \lambda h(\mathbf{w}_{\text{con}}^{(t+1)}) & \leq F(\mathbf{w}_{\text{con}}^{(t)}) + \lambda h(\mathbf{w}_{\text{con}}^{(t)}) \\ & \quad - \frac{\rho C_\gamma^{(t)}}{2} \|\mathbf{w}_{\text{con}}^{(t+1)} - \mathbf{w}_{\text{con}}^{(t)}\|_2^2 \end{aligned} \quad (46)$$

Finally, we complete the proof. ■

Equipped with the two lemmas, we start our proof of Theorem 1. We define some symbols to simplify the expression. Specifically,

$$\begin{aligned}
E_l^{(t)} &= \sum_{i=1}^I f_i(\mathbf{w}_i^{(t)}, \mathbf{w}_{\text{con}}^{(t)}) - f_i(\mathbf{w}_i^{(t+1)}, \mathbf{w}_{\text{con}}^{(t)}) \\
E_c^{(t)} &= \sum_{i=1}^I f_i(\mathbf{w}_i^{(t+1)}, \mathbf{w}_{\text{con}}^{(t)}) + \lambda \|\mathbf{w}_{\text{con}}^{(t)}\|_1 \\
&\quad - \sum_{i=1}^I f_i(\mathbf{w}_i^{(t+1)}, \mathbf{w}_{\text{con}}^{(t+1)}) - \lambda \|\mathbf{w}_{\text{con}}^{(t+1)}\|_1 \\
e_l^{(t)} &= \frac{1}{2\eta_w} \|\mathbf{w}_i^{(t+1)} - \mathbf{w}_i^{(t)}\|_2^2 - \frac{\xi^2}{2\eta_w} \|\mathbf{w}_i^{(t)} - \mathbf{w}_i^{(t-1)}\|_2^2 \\
e_c^{(t)} &= \frac{\rho C_\gamma^{(t)}}{2} \|\mathbf{w}_{\text{con}}^{(t)} - \mathbf{w}_{\text{con}}^{(t+1)}\|_2^2
\end{aligned} \tag{47}$$

Then combining Lemma 1 and Lemma 2, we have

$$\sum_{i=1}^I e_l^{(t)} + e_c^{(t)} \leq E_l^{(t)} + E_c^{(t)}. \tag{48}$$

Summing (48) from 0 to $T-1$, we obtain

$$\begin{aligned}
\sum_{t=0}^{T-1} \sum_{i=1}^I e_l^{(t)} + e_c^{(t)} &\leq \sum_{t=0}^{T-1} E_l^{(t)} + E_c^{(t)} \\
&= \sum_{i=1}^I f_i(\mathbf{w}_i^{(0)}, \mathbf{w}_{\text{con}}^{(0)}) - f_i(\mathbf{w}_i^{(T)}, \mathbf{w}_{\text{con}}^{(T)}) \\
&\quad + \lambda \|\mathbf{w}_{\text{con}}^{(0)}\|_1 - \lambda \|\mathbf{w}_{\text{con}}^{(T)}\|_1 \\
&\leq \sum_{i=1}^I f_i(\mathbf{w}_i^{(0)}, \mathbf{w}_{\text{con}}^{(0)}) - f_i^* + \lambda \|\mathbf{w}_{\text{con}}^{(0)} - \mathbf{w}_{\text{con}}^{(T)}\|_1 \\
&\leq \sum_{i=1}^I f_i(\mathbf{w}_i^{(0)}, \mathbf{w}_{\text{con}}^{(0)}) - f_i^* + \lambda \sqrt{p} \|\mathbf{w}_{\text{con}}^{(0)} - \mathbf{w}_{\text{con}}^{(T)}\|_2 \\
&\leq \sum_{i=1}^I f_i(\mathbf{w}_i^{(0)}, \mathbf{w}_{\text{con}}^{(0)}) - f_i^* + \lambda \sqrt{p} B_r \triangleq \Delta,
\end{aligned} \tag{49}$$

where f_i^* denotes the minimum of f_i . Notice that

$$\begin{aligned}
&\sum_{t=0}^{T-1} e_l^{(t)} \\
&= \sum_{t=0}^{T-1} \left(\frac{1}{2\eta_w} \|\mathbf{w}_i^{(t+1)} - \mathbf{w}_i^{(t)}\|_2^2 - \frac{\xi^2}{2\eta_w} \|\mathbf{w}_i^{(t)} - \mathbf{w}_i^{(t-1)}\|_2^2 \right) \\
&\geq \sum_{t=0}^{T-1} \frac{1 - \xi^2}{2\eta_w} \|\mathbf{w}_i^{(t+1)} - \mathbf{w}_i^{(t)}\|_2^2 - \frac{1}{2\eta_w} \|\mathbf{w}_i^{(0)} - \mathbf{w}_i^{(-1)}\|_2^2 \\
&= \sum_{t=0}^{T-1} \frac{1 - \xi^2}{2\eta_w} \|\mathbf{w}_i^{(t+1)} - \mathbf{w}_i^{(t)}\|_2^2.
\end{aligned} \tag{50}$$

We expand the summation operator to obtain the first inequality. The last equality holds due to initialization conditions of our algorithm. With (49) and (50), we obtain that

$$\frac{1}{T} \sum_{t=0}^{T-1} \sum_{i=1}^I \frac{1 - \xi^2}{2\eta_w} \|\mathbf{w}_i^{(t+1)} - \mathbf{w}_i^{(t)}\|_2^2 + \frac{1}{T} \sum_{t=0}^{T-1} e_c^{(t)} \leq \frac{\Delta}{T}, \tag{51}$$

Since $0 \leq \xi < 1$, we can conclude that

$$\frac{1}{T} \sum_{t=0}^{T-1} \left(\sum_{i=1}^I \|\mathbf{w}_i^{(t+1)} - \mathbf{w}_i^{(t)}\|_2^2 \right) = \frac{C_1}{T}, \tag{52}$$

where $C_1 = \frac{2\Delta\eta_w}{1-\xi^2}$.

In the same way, we obtain that

$$\begin{aligned}
\frac{1}{T} \sum_{t=0}^{T-1} e_c^{(t)} &\leq \frac{\Delta}{T} \\
\Rightarrow \frac{\rho}{2T} \sum_{t=0}^{T-1} C_\gamma^{(t)} \|\mathbf{w}_{\text{con}}^{(t)} - \mathbf{w}_{\text{con}}^{(t+1)}\|_2^2 &\leq \frac{\Delta}{T} \\
\Rightarrow \frac{\rho I \gamma_{\min}}{2T} \sum_{t=0}^{T-1} \|\mathbf{w}_{\text{con}}^{(t)} - \mathbf{w}_{\text{con}}^{(t+1)}\|_2^2 &\leq \frac{\Delta}{T} \\
\Rightarrow \frac{1}{T} \sum_{t=0}^{T-1} \|\mathbf{w}_{\text{con}}^{(t)} - \mathbf{w}_{\text{con}}^{(t+1)}\|_2^2 &\leq \frac{C_2}{T}
\end{aligned} \tag{53}$$

where $C_2 = \frac{2\Delta}{\rho I \gamma_{\min}}$. The third inequality holds since $\gamma_i^{(t)} \geq \gamma_{\min}$ for all i and t .

APPENDIX C PROOF OF THEOREM 2

We will need the following lemma.

Lemma 3. Suppose any two adjacent datasets \mathcal{D}_i and \mathcal{D}'_i of \mathcal{C}_i , let $\mathbf{w}_i^{(t, K_i^{(t)})}$ and $\mathbf{u}_i^{(t, K_i^{(t)})}$ denote the outputs of t -th iteration via the updates (10)-(12) based on \mathcal{D}_i and \mathcal{D}'_i , respectively. The sensitivity of the local update algorithm is $\text{sensitivity} = \max_{\mathcal{D}_i \approx \mathcal{D}'_i} \left\| \mathbf{w}_i^{(t, K_i^{(t)})} - \mathbf{u}_i^{(t, K_i^{(t)})} \right\|_2 \leq 2\eta_w B_f C_s$.

Proof: See supplementary materials for more details. ■

Based on (22), it is not difficult to obtain that

$$\begin{aligned}
\tilde{\mathbf{w}}_i^{(t, K_i^{(t)})} &= \mathbf{w}_{i, \text{ex}}^{(t, K_i^{(t)} - 1)} - \eta_w \left(\nabla g_i \left(\mathbf{w}_{i, \text{ex}}^{(t, K_i^{(t)} - 1)} \right) \right. \\
&\quad \left. + \gamma_i \left(\mathbf{w}_{i, \text{ex}}^{(t, K_i^{(t)} - 1)} - \mathbf{w}_{\text{con}}^{(t)} \right) \right) + \eta_w \mathbf{s}_i^{(t)} \\
&= \check{\mathbf{w}}_i^{(t, K_i^{(t)})} + \eta_w \mathbf{s}_i^{(t)}
\end{aligned} \tag{54}$$

According to [40], if the published $\mathbf{w}_i^{(t+1)}$ is $(\epsilon_i^{(t)}, \delta_i^{(t)})$ -DP, the added noise scale $\sigma_i^{(t)}$ should satisfy (the operator $\text{Proj}_{\mathcal{W}}(\cdot)$ will not increase the sensitivity)

$$\begin{aligned}
\eta_w \sigma_i^{(t)} &\geq \frac{\sqrt{2 \ln(1.25/\delta_i^{(t)})} \cdot \text{sensitivity}}{\epsilon_i^{(t)}} \\
\Rightarrow \sigma_i^{(t)} &\geq \frac{2\sqrt{2 \ln(1.25/\delta_i^{(t)})} B_f C_s}{\epsilon_i^{(t)}},
\end{aligned} \tag{55}$$

Next, for the entire communication rounds, $t = 1, \dots, T$, leveraging the composition results in [44], we conclude that the algorithm $\mathcal{M}_i(\mathcal{S}_i)$ is $(\sum_{t=0}^{T-1} \epsilon_i^{(t)}, \sum_{t=0}^{T-1} \delta_i^{(t)})$ -DP.

APPENDIX D PROOF OF COROLLARY 1

Suppose $\mathbf{z}_{i,j}$ and $\mathbf{z}'_{i,j}$ are the only different record of two adjacent \mathcal{D}_i and \mathcal{D}'_i , respectively. We use \mathbf{w} and \mathbf{u} to denote the outputs via the updates (10)-(12) based on two adjacent datasets \mathcal{D}_i and \mathcal{D}'_i . If $K_i^{(t)} = 1$, we can obtain that $C_s = 1$ directly from the definition of C_s . The sensitivity of the local updates when $K_i^{(t)} = 1$ in t -th communication round is

$$\begin{aligned}
\text{sensitivity} &= \max_{\mathcal{D}_i \approx \mathcal{D}'_i} \left\| \mathbf{w}_i^{(t, 1)} - \mathbf{u}_i^{(t, 1)} \right\|_2 \leq \max_{\mathcal{D}_i \approx \mathcal{D}'_i} \left\| \check{\mathbf{w}}_i^{(t, 1)} - \check{\mathbf{u}}_i^{(t, 1)} \right\|_2 \\
&= \max_{\mathcal{D}_i \approx \mathcal{D}'_i} \left\| (1 - \eta_w \rho \gamma_i^{(0)}) \mathbf{w}_{i, \text{ex}}^{(t, 0)} - \eta_w \nabla g \left(\mathbf{w}_{i, \text{ex}}^{(t, 0)} \right) \right\|_2
\end{aligned}$$

$$\begin{aligned}
& - \left\| \left((1 - \eta_w \rho \gamma_i^{(0)}) \mathbf{u}_{i,\text{ex}}^{(t,0)} - \eta_w \nabla g \left(\mathbf{u}_{i,\text{ex}}^{(t,0)} \right) \right) \right\|_2 \\
& = \max_{\mathcal{D}_i \approx \mathcal{D}'_i} \left\| \eta_w \nabla g \left(\mathbf{u}_{i,\text{ex}}^{(t,0)} \right) - \eta_w \nabla g \left(\mathbf{w}_{i,\text{ex}}^{(t,0)} \right) \right\|_2 \\
& = \max_{\mathcal{D}_i \approx \mathcal{D}'_i} \eta_w \left\| \frac{1}{N_i} \sum_{n=1}^{N_i} \mathbf{z}'_{i,n} - \alpha \mathbf{S}^\top \left(\frac{1}{\mathbf{S} \mathbf{u}_{i,\text{ex}}^{(t,0)} + \zeta \mathbf{1}} \right) + 4\beta \mathbf{u}_{i,\text{ex}}^{(t,0)} \right. \\
& \quad \left. - \left(\frac{1}{N_i} \sum_{n=1}^{N_i} \mathbf{z}_{i,n} - \alpha \mathbf{S}^\top \left(\frac{1}{\mathbf{S} \mathbf{w}_{i,\text{ex}}^{(t,0)} + \zeta \mathbf{1}} \right) + 4\beta \mathbf{w}_{i,\text{ex}}^{(t,0)} \right) \right\|_2 \\
& = \max \frac{\eta_w}{N_i} \|\mathbf{z}'_{i,j} - \mathbf{z}_{i,j}\|_2 \leq \frac{2\eta_w B_z}{N_i}, \tag{56}
\end{aligned}$$

where the first inequality holds due to the non-expansion of the projection operator. The second equality holds due to the updates (10) and (11). The third equality holds since $\mathbf{w}_{i,\text{ex}}^{(t,0)} = \mathbf{u}_{i,\text{ex}}^{(t,0)}$ (the same initial point). The last equality holds since $\mathbf{z}'_{i,j}$ and $\mathbf{z}_{i,j}$ are the only different records in the two datasets. Bringing the sensitivity back to (55), we complete the proof.

REFERENCES

- [1] X. Dong, D. Thanou, M. Rabbat, and P. Frossard, "Learning graphs from data: A signal representation perspective," *IEEE Signal Process. Mag.*, vol. 36, no. 3, pp. 44–63, 2019.
- [2] U. Von Luxburg, "A tutorial on spectral clustering," *Statistics and computing*, vol. 17, pp. 395–416, 2007.
- [3] Z. Wu, S. Pan, F. Chen, G. Long, C. Zhang, and S. Y. Philip, "A comprehensive survey on graph neural networks," *IEEE Trans. Neural Netw. Learn. Syst.*, vol. 32, no. 1, pp. 4–24, 2020.
- [4] G. Mateos, S. Segarra, A. G. Marques, and A. Ribeiro, "Connecting the dots: Identifying network structure via graph signal processing," *IEEE Signal Process. Mag.*, vol. 36, no. 3, pp. 16–43, 2019.
- [5] A. Ortega, P. Frossard, J. Kovačević, J. M. Moura, and P. Vandergheynst, "Graph signal processing: Overview, challenges, and applications," *Proc. IEEE*, vol. 106, no. 5, pp. 808–828, 2018.
- [6] X. Dong, D. Thanou, P. Frossard, and P. Vandergheynst, "Learning Laplacian matrix in smooth graph signal representations," *IEEE Trans. Signal Process.*, vol. 64, no. 23, pp. 6160–6173, 2016.
- [7] V. Kalofolias, "How to learn a graph from smooth signals," in *Proc. Int. Conf. Artif. Intell. Stat., AISTATS*. PMLR, 2016, pp. 920–929.
- [8] X. Pu, T. Cao, X. Zhang, X. Dong, and S. Chen, "Learning to learn graph topologies," *Proc. Adv. Neural Inf. Process. Syst.*, vol. 34, pp. 4249–4262, 2021.
- [9] P. Kairouz, H. B. McMahan, B. Avent, A. Bellet, M. Bennis, A. N. Bhagoji, K. Bonawitz, Z. Charles, G. Cormode, R. Cummings *et al.*, "Advances and open problems in federated learning," *arXiv preprint arXiv:1912.04977*, 2019.
- [10] N. Rieke, J. Hancox, W. Li, F. Milletari, H. R. Roth, S. Albarqouni, S. Bakas, M. N. Galtier, B. A. Landman, K. Maier-Hein *et al.*, "The future of digital health with federated learning," *NPJ Digit. Med.*, vol. 3, no. 1, pp. 1–7, 2020.
- [11] T. Li, A. K. Sahu, A. Talwalkar, and V. Smith, "Federated learning: Challenges, methods, and future directions," *IEEE Signal Process. Mag.*, vol. 37, no. 3, pp. 50–60, 2020.
- [12] T. Yang, X. Yi, J. Wu, Y. Yuan, D. Wu, Z. Meng, Y. Hong, H. Wang, Z. Lin, and K. H. Johansson, "A survey of distributed optimization," *Annu. Rev. Control*, vol. 47, pp. 278–305, 2019.
- [13] P. Kairouz, H. B. McMahan, B. Avent, A. Bellet, M. Bennis, A. N. Bhagoji, K. Bonawitz, Z. Charles, G. Cormode, R. Cummings *et al.*, "Advances and open problems in federated learning," *Found. Trends Mach. Learn.*, vol. 14, no. 1–2, pp. 1–210, 2021.
- [14] B. McMahan, E. Moore, D. Ramage, S. Hampson, and B. A. y Arcas, "Communication-efficient learning of deep networks from decentralized data," in *Proc. Int. Conf. Artif. Intell. Stat., AISTATS*. PMLR, 2017, pp. 1273–1282.
- [15] A. Z. Tan, H. Yu, L. Cui, and Q. Yang, "Towards personalized federated learning," *IEEE Trans. Neural Netw. Learn. Syst.*, 2022.
- [16] Y. Mansour, M. Mohri, J. Ro, and A. T. Suresh, "Three approaches for personalization with applications to federated learning," *arXiv preprint arXiv:2002.10619*, 2020.
- [17] V. Smith, C.-K. Chiang, M. Sanjabi, and A. S. Talwalkar, "Federated multi-task learning," *Proc. Adv. Neural Inf. Process. Syst.*, vol. 30, 2017.
- [18] C. Finn, P. Abbeel, and S. Levine, "Model-agnostic meta-learning for fast adaptation of deep networks," in *Proc. Int. Conf. Mach. Learn. PMLR*, 2017, pp. 1126–1135.
- [19] P. Danaher, P. Wang, and D. M. Witten, "The joint graphical lasso for inverse covariance estimation across multiple classes," *J. R. Stat. Soc. B.*, vol. 76, no. 2, pp. 373–397, 2014.
- [20] P. J. Bickel and E. Levina, "Regularized estimation of large covariance matrices," *Ann. Statist.*, vol. 36, no. 1, p. 199–227, 2008.
- [21] Y. Yuan, D. W. Soh, X. Yang, K. Guo, and T. Q. Quek, "Joint network topology inference via structured fusion regularization," *arXiv preprint arXiv:2103.03471*, 2021.
- [22] X. Zhang and Q. Wang, "Time-varying graph learning under structured temporal priors," in *Proc. Eur. Signal Process. Conf. IEEE*, 2022, pp. 2141–2145.
- [23] K. Yamada, Y. Tanaka, and A. Ortega, "Time-varying graph learning based on sparseness of temporal variation," in *Proc. IEEE Int. Conf. Acoust., Speech, Signal Process.* IEEE, 2019, pp. 5411–5415.
- [24] D. Hallac, Y. Park, S. Boyd, and J. Leskovec, "Network inference via the time-varying graphical lasso," in *Proc. ACM SIGKDD Int. Conf. Knowl. Discov. Data Min.*, 2017, pp. 205–213.
- [25] V. Kalofolias, A. Loukas, D. Thanou, and P. Frossard, "Learning time varying graphs," in *Proc. IEEE Int. Conf. Acoust., Speech, Signal Process.* Ieee, 2017, pp. 2826–2830.
- [26] Z. Li, C. Tang, X. Liu, X. Zheng, W. Zhang, and E. Zhu, "Consensus graph learning for multi-view clustering," *IEEE Trans. Multimedia*, vol. 24, pp. 2461–2472, 2021.
- [27] C. T. Dinh, N. Tran, and J. Nguyen, "Personalized federated learning with moreau envelopes," *Advances in Neural Information Processing Systems*, vol. 33, pp. 21394–21405, 2020.
- [28] A. Bellet, R. Guerraoui, M. Taziki, and M. Tommasi, "Personalized and private peer-to-peer machine learning," in *Proc. Int. Conf. Artif. Intell. Stat., AISTATS*. PMLR, 2018, pp. 473–481.
- [29] O. Marfoq, G. Neglia, A. Bellet, L. Kameni, and R. Vidal, "Federated multi-task learning under a mixture of distributions," *Advances in Neural Information Processing Systems*, vol. 34, pp. 15434–15447, 2021.
- [30] F. Chen, G. Long, Z. Wu, T. Zhou, and J. Jiang, "Personalized federated learning with graph," *arXiv preprint arXiv:2203.00829*, 2022.
- [31] M. Al-Rubaie and J. M. Chang, "Reconstruction attacks against mobile-based continuous authentication systems in the cloud," *IEEE Trans. Inf. Forensics Security*, vol. 11, no. 12, pp. 2648–2663, 2016.
- [32] R. Shokri, M. Stronati, C. Song, and V. Shmatikov, "Membership inference attacks against machine learning models," in *Proc. IEEE Symp. Secur. Privacy (SP)*. IEEE, 2017, pp. 3–18.
- [33] R. Xu, N. Baracaldo, and J. Joshi, "Privacy-preserving machine learning: Methods, challenges and directions," *arXiv preprint arXiv:2108.04417*, 2021.
- [34] C. Dwork, "Differential privacy: A survey of results," in *Proc. Int. Conf. Theory Appl. Models Comput.* Springer, 2008, pp. 1–19.
- [35] L. Stanković, M. Daković, and E. Sejdić, "Introduction to graph signal processing," in *Vertex-Frequency Analysis of Graph Signals*. Springer, 2019, pp. 3–108.
- [36] A. Karaaslanli, S. Saha, S. Aviyente, and T. Maiti, "Multiview graph learning for single-cell rna sequencing data," *bioRxiv*, 2021.
- [37] F. Nie, J. Li, X. Li *et al.*, "Self-weighted multiview clustering with multiple graphs," in *Int. Joint Conf. Artif. Intell.*, 2017, pp. 2564–2570.
- [38] Z. Hu, F. Nie, W. Chang, S. Hao, R. Wang, and X. Li, "Multi-view spectral clustering via sparse graph learning," *Neurocomputing*, vol. 384, pp. 1–10, 2020.
- [39] C. Dwork, F. McSherry, K. Nissim, and A. Smith, "Calibrating noise to sensitivity in private data analysis," in *Proc. Theory of Cryptography Conf.* Springer, 2006, pp. 265–284.
- [40] C. Dwork, A. Roth *et al.*, "The algorithmic foundations of differential privacy," *Found. Trends Theor. Comput. Sci.*, vol. 9, no. 3–4, pp. 211–407, 2014.
- [41] H. B. McMahan, D. Ramage, K. Talwar, and L. Zhang, "Learning differentially private recurrent language models," *arXiv preprint arXiv:1710.06963*, 2017.
- [42] M. Abadi, A. Chu, I. Goodfellow, H. B. McMahan, I. Mironov, K. Talwar, and L. Zhang, "Deep learning with differential privacy," in *Proc. ACM SIGSAC Conf. Comput. Commun. Secur.*, 2016, pp. 308–318.
- [43] S. P. Kasiviswanathan, H. K. Lee, K. Nissim, S. Raskhodnikova, and A. Smith, "What can we learn privately?" *SIAM Journal on Computing*, vol. 40, no. 3, pp. 793–826, 2011.
- [44] P. Kairouz, S. Oh, and P. Viswanath, "The composition theorem for differential privacy," in *Proc. Int. Conf. Mach. Learn.* PMLR, 2015, pp. 1376–1385.

- [45] S. Fortunato, "Community detection in graphs," *Phys. Rep.*, vol. 486, no. 3-5, pp. 75–174, 2010.
- [46] J. Han, J. Pei, and M. Kamber, *Data mining: concepts and techniques*. Elsevier, 2011.
- [47] S. Chen, A. Sandryhaila, G. Lederman, Z. Wang, J. M. Moura, P. Rizzo, J. Biela, J. H. Garrett, and J. Kovačević, "Signal inpainting on graphs via total variation minimization," in *Proc. IEEE Int. Conf. Acoust., Speech, Signal Process.* IEEE, 2014, pp. 8267–8271.
- [48] R. K. Kana, L. E. Libero, and M. S. Moore, "Disrupted cortical connectivity theory as an explanatory model for autism spectrum disorders," *Phys. Life Rev.*, vol. 8, no. 4, pp. 410–437, 2011.
- [49] S. S. Saboksayr, G. Mateos, and M. Cetin, "Online discriminative graph learning from multi-class smooth signals," *Signal Process.*, vol. 186, p. 108101, 2021.

Supplementary Materials

A. Derivation of the inverse distance schema (16)

The derivation is inspired by [37], and we first define an auxiliary problem [37]

$$\min_{\mathbf{w}_{\text{con}}} \sum_{i=1}^I \frac{\rho}{2} \|\mathbf{w}_i^{(t+1)} - \mathbf{w}_{\text{con}}\|_2 + \lambda \|\mathbf{w}_{\text{con}}\|_1. \quad (57)$$

Note that no weight factors γ_i are explicitly defined in (57). If we take the derivative of (57) w.r.t. \mathbf{w}_{con} and set it to zero, we can obtain

$$\frac{\rho}{2} \sum_{i=1}^I \tilde{\gamma}_i \frac{\partial \|\mathbf{w}_i^{(t+1)} - \mathbf{w}_{\text{con}}\|_2}{\partial \mathbf{w}_{\text{con}}} + \frac{\partial \|\mathbf{w}_{\text{con}}\|_1}{\partial \mathbf{w}_{\text{con}}} = \mathbf{0}, \quad (58)$$

where

$$\tilde{\gamma}_i = \frac{1}{2\|\mathbf{w}_i^{(t+1)} - \mathbf{w}_{\text{con}}\|_2}. \quad (59)$$

It is observed that (58) is dependent on \mathbf{w}_{con} , which means that $\tilde{\gamma}_i$ and \mathbf{w}_{con} are coupled with each other. However, we can alternately update \mathbf{w}_{con} and $\tilde{\gamma}_i$ to solve (57). First, we assume $\tilde{\gamma}_i$ is stationary, (58) is the same as the derivative of the problem (13), and $\tilde{\gamma}_i$ can be viewed as $\gamma_i^{(t)}$ in (13). After updating \mathbf{w}_{con} from (13), we adjust $\gamma_i^{(t)}$ correspondingly using (59). In this way, we finally solve (57), and at the same time obtain adjustable weights.

B. Proof of Theorem 3

Similar to the proof of Theorem 1, we assume $K_i^{(t)} = 1$ to simplify notations. We first provide the following lemma.

Lemma 4. Suppose that Assumptions 1-3 hold, for any client C_i , the updated $\mathbf{w}_i^{(t+1)}$ satisfies that

$$\begin{aligned} f_i(\mathbf{w}_i^{(t+1)}, \mathbf{w}_{\text{con}}^{(t)}) &\leq f_i(\mathbf{w}_i^{(t)}, \mathbf{w}_{\text{con}}^{(t)}) - \frac{1}{2\eta_w} \|\mathbf{w}_i^{(t+1)} - \mathbf{w}_i^{(t)}\|_2^2 \\ &+ \frac{\xi^2}{2\eta_w} \|\mathbf{w}_i^{(t)} - \mathbf{w}_i^{(t-1)}\|_2^2 + \|\mathbf{s}_i^{(t)}\|_2 \left(\xi B_r + \eta_w (B_f + \|\mathbf{s}_i^{(t)}\|_2) \right) \end{aligned} \quad (60)$$

Proof: Similar to (38), we have

$$\begin{aligned} &f_i(\mathbf{w}_i^{(t+1)}, \mathbf{w}_{\text{con}}^{(t)}) \\ &\leq f_i(\mathbf{w}_i^{(t)}, \mathbf{w}_{\text{con}}^{(t)}) + \left\langle \nabla_{\mathbf{w}_i} f_i(\mathbf{w}_{i,\text{ex}}^{(t)}, \mathbf{w}_{\text{con}}^{(t)}), \mathbf{w}_i^{(t+1)} - \mathbf{w}_i^{(t)} \right\rangle \\ &\quad + \frac{1}{2\eta_w} \|\mathbf{w}_i^{(t+1)} - \mathbf{w}_{i,\text{ex}}^{(t)}\|_2^2 \\ &\leq f_i(\mathbf{w}_i^{(t)}, \mathbf{w}_{\text{con}}^{(t)}) + \frac{1}{2\eta_w} \|\mathbf{w}_i^{(t+1)} - \mathbf{w}_{i,\text{ex}}^{(t)}\|_2^2 \\ &\quad + \left\langle \mathbf{s}_i^{(t)} + \frac{1}{\eta_w} (\mathbf{w}_i^{(t+1)} - \mathbf{w}_{i,\text{ex}}^{(t)}), \mathbf{w}_i^{(t)} - \mathbf{w}_i^{(t+1)} \right\rangle \\ &\leq f_i(\mathbf{w}_i^{(t)}, \mathbf{w}_{\text{con}}^{(t)}) - \frac{1}{2\eta_w} \|\mathbf{w}_i^{(t+1)} - \mathbf{w}_i^{(t)}\|_2^2 \\ &\quad + \|\mathbf{s}_i^{(t)}\|_2 \|\mathbf{w}_i^{(t+1)} - \mathbf{w}_i^{(t)}\|_2 + \frac{1}{2\eta_w} \|\mathbf{w}_i^{(t)} - \mathbf{w}_{i,\text{ex}}^{(t)}\|_2^2 \\ &= f_i(\mathbf{w}_i^{(t)}, \mathbf{w}_{\text{con}}^{(t)}) + \|\mathbf{s}_i^{(t)}\|_2 \|\mathbf{w}_i^{(t)} - \mathbf{w}_{i,\text{ex}}^{(t)} + \mathbf{w}_{i,\text{ex}}^{(t)} - \mathbf{w}_i^{(t+1)}\|_2 \\ &\quad - \frac{1}{2\eta_w} \|\mathbf{w}_i^{(t+1)} - \mathbf{w}_i^{(t)}\|_2^2 + \frac{\xi^2}{2\eta_w} \|\mathbf{w}_i^{(t)} - \mathbf{w}_i^{(t-1)}\|_2^2 \\ &\leq f_i(\mathbf{w}_i^{(t)}, \mathbf{w}_{\text{con}}^{(t)}) - \frac{1}{2\eta_w} \|\mathbf{w}_i^{(t+1)} - \mathbf{w}_i^{(t)}\|_2^2 \\ &\quad + \|\mathbf{s}_i^{(t)}\|_2 \left(\|\mathbf{w}_i^{(t)} - \mathbf{w}_{i,\text{ex}}^{(t)}\|_2 + \|\mathbf{w}_{i,\text{ex}}^{(t)} - \mathbf{w}_i^{(t+1)}\|_2 \right) \end{aligned}$$

$$\begin{aligned} &+ \frac{\xi^2}{2\eta_w} \|\mathbf{w}_i^{(t)} - \mathbf{w}_i^{(t-1)}\|_2^2 \\ &\leq f_i(\mathbf{w}_i^{(t)}, \mathbf{w}_{\text{con}}^{(t)}) - \frac{1}{2\eta_w} \|\mathbf{w}_i^{(t+1)} - \mathbf{w}_i^{(t)}\|_2^2 \\ &\quad + \frac{\xi^2}{2\eta_w} \|\mathbf{w}_i^{(t)} - \mathbf{w}_i^{(t-1)}\|_2^2 + \|\mathbf{s}_i^{(t)}\|_2 \left(\xi \|\mathbf{w}_i^{(t)} - \mathbf{w}_i^{(t-1)}\|_2 \right. \\ &\quad \left. + \eta_w \|\nabla_{\mathbf{w}_i} f(\mathbf{w}_{i,\text{ex}}^{(t)}, \mathbf{w}_{\text{con}}^{(t)}) + \mathbf{s}_i^{(t)}\|_2 \right) \\ &\leq f_i(\mathbf{w}_i^{(t)}, \mathbf{w}_{\text{con}}^{(t)}) + \|\mathbf{s}_i^{(t)}\|_2 \left(\xi B_r + \eta_w (B_f + \|\mathbf{s}_i^{(t)}\|_2) \right) \\ &\quad - \frac{1}{2\eta_w} \|\mathbf{w}_i^{(t+1)} - \mathbf{w}_i^{(t)}\|_2^2 + \frac{\xi^2}{2\eta_w} \|\mathbf{w}_i^{(t)} - \mathbf{w}_i^{(t-1)}\|_2^2, \end{aligned} \quad (61)$$

where the second inequality holds due to that updating (22)-(23) satisfies the following first-order optimality condition for all $\mathbf{y} \in \mathcal{W}$.

$$\left\langle \nabla_{\mathbf{w}_i} f_i(\mathbf{w}_{i,\text{ex}}^{(t)}, \mathbf{w}_{\text{con}}^{(t)}) + \frac{1}{\eta_w} (\mathbf{w}_i^{(t+1)} - \mathbf{w}_{i,\text{ex}}^{(t)}) + \mathbf{s}_i^{(t)}, \mathbf{y} - \mathbf{w}_i^{(t+1)} \right\rangle \geq 0. \quad (62)$$

The third inequality holds for the same reason as that of proof of Theorem 1. The fifth inequality holds due to the update procedure of our algorithm and the non-expansiveness of the projection operator. The last inequality holds due to Assumption 2 and (34). Finally, we complete the proof. ■

With Lemma 4, we next define

$$\begin{aligned} \tilde{E}_l^{(t)} &= \sum_{i=1}^I \mathbb{E} \left[f_i(\mathbf{w}_i^{(t)}, \mathbf{w}_{\text{con}}^{(t)}) \right] - \mathbb{E} \left[f_i(\mathbf{w}_i^{(t+1)}, \mathbf{w}_{\text{con}}^{(t)}) \right] \\ \tilde{E}_c^{(t)} &= \sum_{i=1}^I \mathbb{E} \left[f_i(\mathbf{w}_i^{(t+1)}, \mathbf{w}_{\text{con}}^{(t)}) \right] + \lambda \mathbb{E} [\|\mathbf{w}_{\text{con}}^{(t)}\|_1] \\ &\quad - \sum_{i=1}^I \mathbb{E} \left[f_i(\mathbf{w}_i^{(t+1)}, \mathbf{w}_{\text{con}}^{(t+1)}) \right] - \lambda \mathbb{E} [\|\mathbf{w}_{\text{con}}^{(t+1)}\|_1] \\ \tilde{e}_l^{(t)} &= \frac{1}{2\eta_w} \mathbb{E} [\|\mathbf{w}_i^{(t+1)} - \mathbf{w}_i^{(t)}\|_2^2] - \frac{\xi^2}{2\eta_w} \mathbb{E} [\|\mathbf{w}_i^{(t)} - \mathbf{w}_i^{(t-1)}\|_2^2] \\ \tilde{e}_c^{(t)} &= \frac{\rho C_\gamma^{(t)}}{2} \mathbb{E} [\|\mathbf{w}_{\text{con}}^{(t)} - \mathbf{w}_{\text{con}}^{(t+1)}\|_2^2] \\ C_s^{(t)} &= \mathbb{E} [\|\mathbf{s}_i^{(t)}\|_2 (\xi B_r + \eta_w (B_f + \|\mathbf{s}_i^{(t)}\|_2))] \end{aligned} \quad (63)$$

Following the same way of (49), we have

$$\begin{aligned} &\sum_{t=0}^{T-1} \sum_{i=1}^I \tilde{e}_l^{(t)} + \tilde{e}_c^{(t)} - C_s^{(t)} \\ &\leq \sum_{t=0}^{T-1} \tilde{E}_l^{(t)} + \tilde{E}_c^{(t)} \\ &= \sum_{i=1}^I \mathbb{E} \left[f_i(\mathbf{w}_i^{(0)}, \mathbf{w}_{\text{con}}^{(0)}) \right] - \mathbb{E} \left[f_i(\mathbf{w}_i^{(T)}, \mathbf{w}_{\text{con}}^{(T)}) \right] \\ &\quad + \lambda \mathbb{E} [\|\mathbf{w}_{\text{con}}^{(0)}\|_1] - \lambda \mathbb{E} [\|\mathbf{w}_{\text{con}}^{(T)}\|_1] \\ &\leq \sum_{i=1}^I \mathbb{E} \left[f_i(\mathbf{w}_i^{(0)}, \mathbf{w}_{\text{con}}^{(0)}) \right] - f_i^{\min} + \lambda \mathbb{E} [\|\mathbf{w}_{\text{con}}^{(0)} - \mathbf{w}_{\text{con}}^{(T)}\|_1] \\ &\leq \sum_{i=1}^I f_i(\mathbf{w}_i^{(0)}, \mathbf{w}_{\text{con}}^{(0)}) - f_i^{\min} + \lambda \sqrt{p} B_r = \Delta, \end{aligned} \quad (64)$$

We remove the expectation operator in the last inequality since $\mathbf{w}_i^{(0)}$ and $\mathbf{w}_{\text{con}}^{(0)}$ are deterministic. Furthermore, following (50), we have

$$\sum_{t=0}^{T-1} \tilde{e}_i^{(t)} \geq \sum_{t=0}^{T-1} \frac{1-\xi^2}{2\eta_w} \mathbb{E} \left[\|\mathbf{w}_i^{(t+1)} - \mathbf{w}_i^{(t)}\|_2^2 \right]. \quad (65)$$

We can also yield that

$$\begin{aligned} & \sum_{t=0}^{T-1} \left(\sum_{i=1}^I \mathbb{E} \left[\|\mathbf{s}_i^{(t)}\|_2 \left(\xi B_r + \eta_w (B_f + \|\mathbf{s}_i^{(t)}\|_2) \right) \right] \right) \\ &= \sum_{t=0}^{T-1} \left(\sum_{i=1}^I (\xi B_r + \eta_w B_f) \mathbb{E} \left[\|\mathbf{s}_i^{(t)}\|_2 \right] \right) \\ &+ \sum_{t=0}^{T-1} \left(\sum_{i=1}^I \eta_w \mathbb{E} \left[\|\mathbf{s}_i^{(t)}\|_2^2 \right] \right) \\ &= \sqrt{p} (\xi B_r + \eta_w B_f) T I \sigma + p T I \eta_w \sigma^2 \end{aligned} \quad (66)$$

Equipped with (64), (65) and (66), we reach that

$$\begin{aligned} & \frac{1}{T} \sum_{t=0}^{T-1} \sum_{i=1}^I \frac{1-\xi^2}{2\eta_w} \mathbb{E} \left[\|\mathbf{w}_i^{(t+1)} - \mathbf{w}_i^{(t)}\|_2^2 \right] + \frac{1}{T} \sum_{t=0}^{T-1} \tilde{e}_c^{(t)} \\ &\leq \frac{\Delta}{T} + \sqrt{p} (\xi B_r + \eta_w B_f) I \sigma + p I \eta_w \sigma^2. \end{aligned} \quad (67)$$

Therefore, we can easily conclude that

$$\begin{aligned} & \frac{1}{T} \sum_{t=0}^{T-1} \sum_{i=1}^I \mathbb{E} \left[\|\mathbf{w}_i^{(t+1)} - \mathbf{w}_i^{(t)}\|_2^2 \right] \\ &\leq \frac{2\eta_w \Delta}{(1-\xi^2)T} + \frac{2\sqrt{p}\eta_w I \sigma (\xi B_r + \eta_w B_f) + 2pI\eta_w^2 \sigma^2}{1-\xi^2} \\ &= \frac{C_1}{T} + \Delta_1 \\ & \frac{1}{T} \sum_{t=0}^{T-1} \mathbb{E} \left[\|\mathbf{w}_{\text{con}}^{(t)} - \mathbf{w}_{\text{con}}^{(t+1)}\|_2^2 \right] \\ &\leq \frac{2\Delta}{\rho I \gamma_{\min} T} + \frac{2\sqrt{p}\sigma (\xi B_r + \eta_w B_f) + 2p\eta_w \sigma^2}{\rho \gamma_{\min}} \\ &= \frac{C_2}{T} + \Delta_2. \end{aligned} \quad (68)$$

C. Proof of Lemma 3

To prove Lemma 3, we first provide the following lemma.

Lemma 5. For $a, b > 0$, if the sequences $v^{(1)}, \dots, v^{(K)}$ satisfy

$$\begin{aligned} v^{(k)} &= av^{(k-1)} + bv^{(k-2)} \\ v^{(1)} &= v_1, \quad v^{(2)} = v_2, \end{aligned} \quad (70)$$

then we have

$$\begin{aligned} \sum_{k=1}^{K-1} v^{(k)} &= \frac{rv_1 - v_2}{(s+r)(1+s)} (1 - (-s)^{K-1}) \\ &+ \frac{sv_1 + v_2}{(s+r)(1-r)} (1 - r^{K-1}), \end{aligned} \quad (71)$$

where

$$s = \frac{-a - \sqrt{a^2 + 4b}}{2}, \quad r = \frac{a - \sqrt{a^2 + 4b}}{2}. \quad (72)$$

Proof: From (70), we have that

$$v^{(k)} + sv^{(k-1)} = (a+s)v^{(k-1)} + bv^{(k-2)}. \quad (73)$$

If $s = \frac{b}{a+s}$, i.e., $s = \frac{-a \pm \sqrt{a^2 + 4b}}{2}$, we obtain that

$$v^{(k)} + sv^{(k-1)} = (a+s)(v^{(k-1)} + sv^{(k-2)}). \quad (74)$$

Let us set $s = \frac{-a - \sqrt{a^2 + 4b}}{2}$, and we reach that

$$v^{(k)} + sv^{(k-1)} = r(v^{(k-1)} + sv^{(k-2)}), \quad (75)$$

where $r = \frac{a - \sqrt{a^2 + 4b}}{2}$. We can observe from (75) that $v^{(k)} + sv^{(k-1)}$ is a geometric sequence, i.e.,

$$v^{(k)} + sv^{(k-1)} = r^{k-2} (v_2 + sv_1) \quad (76)$$

Based on (76), we then construct the following recursive formula

$$\begin{aligned} v^{(k)} + s_1 r^{k-1} &= s_2 (v^{(k-1)} + s_1 r^{k-2}) \\ \implies v^{(k)} - s_2 v^{(k-1)} &= (s_1 s_2 - r s_1) r^{k-2}. \end{aligned} \quad (77)$$

If we let $s_1 = \frac{-sv_1 - v_2}{s+r}$ and $s_2 = -s$, we have

$$v^{(k)} - \frac{sv_1 + v_2}{s+r} r^{k-1} = (-s) \left(v^{(k-1)} - \frac{sv_1 + v_2}{s+r} r^{k-2} \right), \quad (78)$$

which is also a geometric sequence. It is not difficult to conclude that

$$\begin{aligned} v^{(k)} - \frac{sv_1 + v_2}{s+r} r^{k-1} &= (-s)^{k-1} \left(v_1 - \frac{sv_1 + v_2}{s+r} \right) \\ \implies v^{(k)} &= \left(v_1 - \frac{sv_1 + v_2}{s+r} \right) (-s)^{k-1} + \frac{sv_1 + v_2}{s+r} r^{k-1}. \end{aligned} \quad (79)$$

Therefore, $v^{(k)}$ is a summation of two geometric sequences. Based on the geometric sum formula, we finally obtain that

$$\begin{aligned} \sum_{k=1}^{K-1} v^{(k)} &= \frac{rv_1 - v_2}{(s+r)(1+s)} (1 - (-s)^{K-1}) \\ &+ \frac{sv_1 + v_2}{(s+r)(1-r)} (1 - r^{K-1}). \end{aligned} \quad (80)$$

■

With Lemma 5, we provide our proof for Lemma 3. For one communication between client \mathcal{C}_i and the central server, the sensitivity of the updates in \mathcal{C}_i is

sensitivity

$$= \max_{\mathcal{D}_i \approx \mathcal{D}'_i} \left\| \mathbf{w}_i^{(t, K_i^{(t)})} - \mathbf{u}_i^{(t, K_i^{(t)})} \right\|_2 \quad (81a)$$

$$= \max_{\mathcal{D}_i \approx \mathcal{D}'_i} \left\| \text{Proj}_{\mathcal{W}} \left(\check{\mathbf{w}}_i^{(t, K_i^{(t)})} \right) - \text{Proj}_{\mathcal{W}} \left(\check{\mathbf{u}}_i^{(t, K_i^{(t)})} \right) \right\|_2 \quad (81b)$$

$$\leq \max_{\mathcal{D}_i \approx \mathcal{D}'_i} \left\| \check{\mathbf{w}}_i^{(t, K_i^{(t)})} - \check{\mathbf{u}}_i^{(t, K_i^{(t)})} \right\|_2 \quad (81c)$$

$$\begin{aligned} &= \max_{\mathcal{D}_i \approx \mathcal{D}'_i} \left\| c_1^{(1)} \mathbf{w}_i^{(t, K_i^{(t)}-1)} - c_2^{(1)} \mathbf{w}_i^{(t, K_i^{(t)}-2)} - \eta_w \nabla g \left(\mathbf{w}_{i, \text{ex}}^{(t, K_i^{(t)}-1)} \right) \right. \\ &\quad \left. - \left(c_1^{(1)} \mathbf{u}_i^{(t, K_i^{(t)}-1)} - c_2^{(1)} \mathbf{u}_i^{(t, K_i^{(t)}-2)} - \eta_w \nabla g \left(\mathbf{u}_{i, \text{ex}}^{(t, K_i^{(t)}-1)} \right) \right) \right\|_2 \end{aligned} \quad (81d)$$

$$\begin{aligned}
&\leq \max_{\mathcal{D}_i \approx \mathcal{D}'_i} c_1^{(1)} \left\| \mathbf{w}_i^{(t, K_i^{(t)}-1)} - \mathbf{u}_i^{(t, K_i^{(t)}-1)} \right\|_2 \\
&\quad + c_2^{(1)} \left\| \mathbf{w}_i^{(t, K_i^{(t)}-2)} - \mathbf{u}_i^{(t, K_i^{(t)}-2)} \right\|_2 \\
&\quad + \eta_w \left\| \nabla g \left(\mathbf{w}_{i, \text{ex}}^{(t, K_i^{(t)}-1)} \right) - \nabla g \left(\mathbf{u}_{i, \text{ex}}^{(t, K_i^{(t)}-1)} \right) \right\|_2 \quad (81e)
\end{aligned}$$

$$\begin{aligned}
&\leq \max_{\mathcal{D}_i \approx \mathcal{D}'_i} c_1^{(2)} \left\| \mathbf{w}_i^{(t, K_i^{(t)}-2)} - \mathbf{u}_i^{(t, K_i^{(t)}-2)} \right\|_2 \\
&\quad + c_2^{(2)} \left\| \mathbf{w}_i^{(t, K_i^{(t)}-3)} - \mathbf{u}_i^{(t, K_i^{(t)}-3)} \right\|_2 \\
&\quad + \eta_w \sum_{k=0}^1 c_1^{(k)} \left\| \nabla g \left(\mathbf{w}_{i, \text{ex}}^{(t, K_i^{(t)}-k-1)} \right) \right. \\
&\quad \quad \left. - \nabla g \left(\mathbf{u}_{i, \text{ex}}^{(t, K_i^{(t)}-k-1)} \right) \right\|_2 \quad (81f)
\end{aligned}$$

$$\begin{aligned}
&\leq \max_{\mathcal{D}_i \approx \mathcal{D}'_i} c_1^{(K_i^{(t)}-1)} \left\| \mathbf{w}_i^{(t, 0)} - \mathbf{u}_i^{(t, 0)} \right\|_2 \\
&\quad + c_2^{(K_i^{(t)}-1)} \left\| \mathbf{w}_i^{(t, -1)} - \mathbf{u}_i^{(t, -1)} \right\|_2 \\
&\quad + \eta_w \sum_{k=0}^{K_i^{(t)}-1} c_1^{(k)} \left\| \nabla g \left(\mathbf{w}_{i, \text{ex}}^{(t, K_i^{(t)}-k-1)} \right) \right. \\
&\quad \quad \left. - \nabla g \left(\mathbf{u}_{i, \text{ex}}^{(t, K_i^{(t)}-k-1)} \right) \right\|_2 \quad (81g)
\end{aligned}$$

$$\begin{aligned}
&= \max_{\mathcal{D}_i \approx \mathcal{D}'_i} \eta_w \sum_{k=0}^{K_i^{(t)}-1} c_1^{(k)} \left\| \nabla g \left(\mathbf{w}_{i, \text{ex}}^{(t, K_i^{(t)}-k-1)} \right) \right. \\
&\quad \quad \left. - \nabla g \left(\mathbf{u}_{i, \text{ex}}^{(t, K_i^{(t)}-k-1)} \right) \right\|_2 \quad (81h)
\end{aligned}$$

$$\leq 2\eta_w B_f \sum_{k=0}^{K_i^{(t)}-1} c_1^{(k)} \quad (81i)$$

$$\begin{aligned}
&= 2\eta_w B_f \left(\frac{rc_1^{(1)} - c_1^{(2)}}{(s+r)(1+s)} \left(1 - (-s)^{K_i^{(t)}-1} \right) \right. \\
&\quad \quad \left. + \frac{sc_1^{(1)} + c_1^{(2)}}{(s+r)(1-r)} \left(1 - r^{K_i^{(t)}-1} \right) + 1 \right) \quad (81j)
\end{aligned}$$

$$\triangleq 2\eta_w B_f C_s,$$

where s and r are defined as Lemma 5, and $a = (1 + \xi)(1 - \eta_w \rho \gamma_i^{(t)})$, $b = \xi(1 - \eta_w \rho \gamma_i^{(t)})$ in our algorithm. The inequality (81c) holds due to the non-expansion of the projection operator $\text{Proj}_{\mathcal{W}}$. The inequality (81d) holds due to the recursive derivation based on (10) and (11), where $c_1^{(1)} = a$ and $c_2^{(1)} = b$. The inequalities (81f)-(81g) hold since we repeat the derivation (81a)-(81e) up to the initial points, where $c_1^{(k)}$ and $c_2^{(k)}$ are the coefficient sequences. It is not difficult to check that the sequences satisfy

$$\begin{aligned}
c_1^{(k)} &= ac_1^{(k-1)} + c_2^{(k-1)} \\
c_2^{(k)} &= bc_1^{(k-1)} \\
c_1^{(1)} &= a, \quad c_1^{(2)} = a^2 + b. \quad (82)
\end{aligned}$$

Thus, $c_1^{(1)}, \dots, c_1^{(k)}$ is the sequence described in Lemma 5. The equality (81h) holds since we assume the initial points are equal. The inequality (81i) holds due to the definition of B_f in Proposition 1. Finally, we can directly use the results of Lemma 5 to obtain (81j).